INVESTIGATING 50 YEARS (1974 – 2024) OF NATURAL AND PLANNED VEGETATION EXPANSION AT TORONTO'S LESLIE STREET SPIT USING LANDSAT IMAGERY

by

Emma Hauser

Bachelor of Applied Science, 2020, University of Toronto

A major research paper presented to

Toronto Metropolitan University

in partial fulfillment of the requirements for the degree of

Master of Spatial Analysis

in the program of Spatial Analysis

Toronto, Ontario, Canada, 2026

AUTHOR'S DECLARATION FOR ELECTRONIC SUBMISSION OF AN MRP

I hereby declare that I am the sole author of this MRP. This is a true copy of the MRP, including any required final revisions.

I authorize Toronto Metropolitan University to lend this MRP to other institutions or individuals for the purpose of scholarly research.

I further authorize Toronto Metropolitan University to reproduce this MRP by photocopying or by other means, in total or in part, at the request of other institutions or individuals for the purpose of scholarly research.

I understand that my MRP may be made electronically available to the public.

ABSTRACT

The Leslie Street Spit is a constructed peninsula on the Toronto waterfront in Ontario, Canada. Natural processes that evolved during the planning and construction of the site shaped the Spit into a unique "accidental wilderness." As a result, the Toronto and Region Conservation Authority developed a plan to create, enhance, and restore habitats. In this research, remotely sensed data are used to investigate vegetation expansion at the Leslie Street Spit. Landsat-1 through Landsat-9 provided 12 images over a 50-year period (1974 to 2024) that formed nine image pairs for comparison over variable time intervals. Principal Components, the Tasseled Cap Transformation, the Normalized Difference Vegetation Index, and Image Texture were derived for use as additional input parameters in unsupervised land cover classification procedures. They proved valuable in accounting for and distinguishing greenness in the imagery. Land cover classifications were combined in an image differencing change detection process that allowed for the monitoring of vegetation change. Over the 50-year study period, the total area of vegetation expansion was estimated to be 213 ha (2,128,725 m^2), at an average annual rate of 4.26 ha/year. From 1974 to 1995, when natural succession was the mechanism for vegetation expansion, approximately 84.8 ha (847,800 m^2) of vegetation expansion occurred, at an average annual rate of 4.04 ha/year. From 1995 to 2024, when natural succession as well as habitat enhancement accounted for vegetation expansion, approximately 128 ha (1,280,925 m^2) of growth occurred, at an average annual rate of 4.42 ha/year.

ACKNOWLEDGMENTS

I would like to express my sincere gratitude to my supervisor, Dr. Wayne Forsythe, for his guidance, insight, and mentorship at every stage of this research. I am deeply thankful to my husband, Alex, for his unwavering care and support. I would like to thank my parents for their constant encouragement and for instilling a profound appreciation for the miraculous Leslie Street Spit and Toronto geography in general through summer bicycling trips. Finally, I would like to extend my gratitude to the Toronto Metropolitan University Department of Geography and Environmental Studies and the Spatial Analysis program faculty – this program has strengthened my geospatial research skills and provided an opportunity to explore a favourite study area in-depth using remote sensing and GIS applications.

CONTENTS

LIST OF TABLES

LIST OF FIGURES

LIST OF ACRONYMS

ASTER – Advanced Spaceborne Thermal Emission and Reflection Radiometer

CASI – Compact Airborne Spectrographic Imager

GIS – Geographic Information Systems

GLCM – Grey Level Co-occurrence Matrix

GWPCA – Geographically Weighted Principal Component Analysis

ISODATA – Iterative Self-Organizing Data Analysis Techniques

MODIS – Moderate Resolution Imaging Spectroradiometer

MSS – Multispectral Scanner

NAD – North American Datum

NDVI – Normalized Difference Vegetation Index

NIR – Near-Infrared

OLI – Operational Land Imager

PALSAR – Phased Array L-band Synthetic Aperture Radar

PCA – Principal Component Analysis

PCIDSK – PCI Geomatics Database File

PS2 – PlanetScope

SPOT – Satellite Pour L'Observation de la Terre

TRCA – Toronto and Region Conservation Authority

TM – Thematic Mapper

USGS – United States Geological Survey

UTM – Universal Transverse Mercator

WRS – World Reference System

1. INTRODUCTION

1.1 Remote Sensing for Change Detection

Remotely sensed imagery, spatial technologies, and computer processing are useful for monitoring environmental change and trends, according to Forsythe et al. (2012), who studied drought-induced changes in water surface area in Lake Mead (USA). Coppin and Bauer (1996) assert that digital change detection involves "the quantification of temporal phenomena from multidate imagery that is most commonly acquired by satellite-based multispectral sensors." Satellite-based technologies facilitate change measurement over wide areas as well as pattern detection (Forsythe et al., 2012). Shen et al. (2019) mapped the spatial distribution of afforestation in Guangdong, China, using Landsat and Phased Array L-band Synthetic Aperture Radar (PALSAR) data. They agree that remotely sensed time series data have been an effective spatial detection tool for monitoring long-term vegetation changes. Conventional methods of vegetation mapping to identify expansion/reduction dynamics by field surveys are financially costly, human resource-intense, and challenging in rugged areas; the growing variety and availability of remotely sensed data (often freely accessible) as well as advanced data processing technologies allow information on vegetation expansion to be obtained at different scales and at a low cost (Mancino et al., 2025).

Mancino et al. (2025) compared various change detection techniques to assess natural forest expansion in the Mediterranean Basin using Landsat data. They describe three main groups of change detection techniques: visual interpretation (time-consuming, as changes are identified by analyzing the shape, tone, texture, pattern, size, and association of various objects), object-based (proposed more recently, combining visual interpretation and quantitative aspects, taking into account the similarity of contiguous pixels), and pixel-based (most widely used) methods. Pixel-based methods represent the best-performing change detection technique, according to Mancino

et al. (2025). Within this category are two common approaches: (1) image difference classification using the single spectral bands, or more commonly, an index derived from a combination of bands such as the Normalized Difference Vegetation Index (NDVI); or (2) a post-classification ("delta") approach involving a comparison of independently classified images from two dates (Mancino et al., 2025).

Mancino et al. (2014) used the NDVI differencing method to assess natural expansion of forests in the Basilicata region of Italy. They emphasize that anthropogenic and naturally induced land cover changes affect the spatial and temporal distribution of environmental resources, altering ecosystem composition and productivity. The availability of land cover data at different spatial and temporal scales encourages the development and implementation of vegetation change detection techniques, furthering understanding of vegetation and ecosystem dynamics (Mancino et al., 2014).

1.2 Study Area

The Leslie Street Spit (Figure 1), otherwise known as the Outer Harbour Headland and now home to Tommy Thompson Park, is a constructed peninsula on the Toronto waterfront, currently over 500 hectares in area and extends five kilometres into Lake Ontario (Hough, 2004). It was engineered from construction-site concrete, earth fill, and dredged sand, starting in 1959, to create land for port-related infrastructure and to accommodate increased shipping expected from the St. Lawrence Seaway (Hough, 2004). In the early 1970s, it became clear that a site for port facilities was no longer needed, but by this time, natural processes that evolved during the planning and construction of the site shaped the Spit into a unique "accidental wilderness." This prompted the Toronto and Region Conservation Authority (TRCA) to develop a plan for aquatic and terrestrial habitat enhancement (TRCA, 2020). The land base of the Spit increased significantly between 1974 and 1983. Meadows, forests, woodlands, thickets, beaches, wetlands, and aquatic habitats

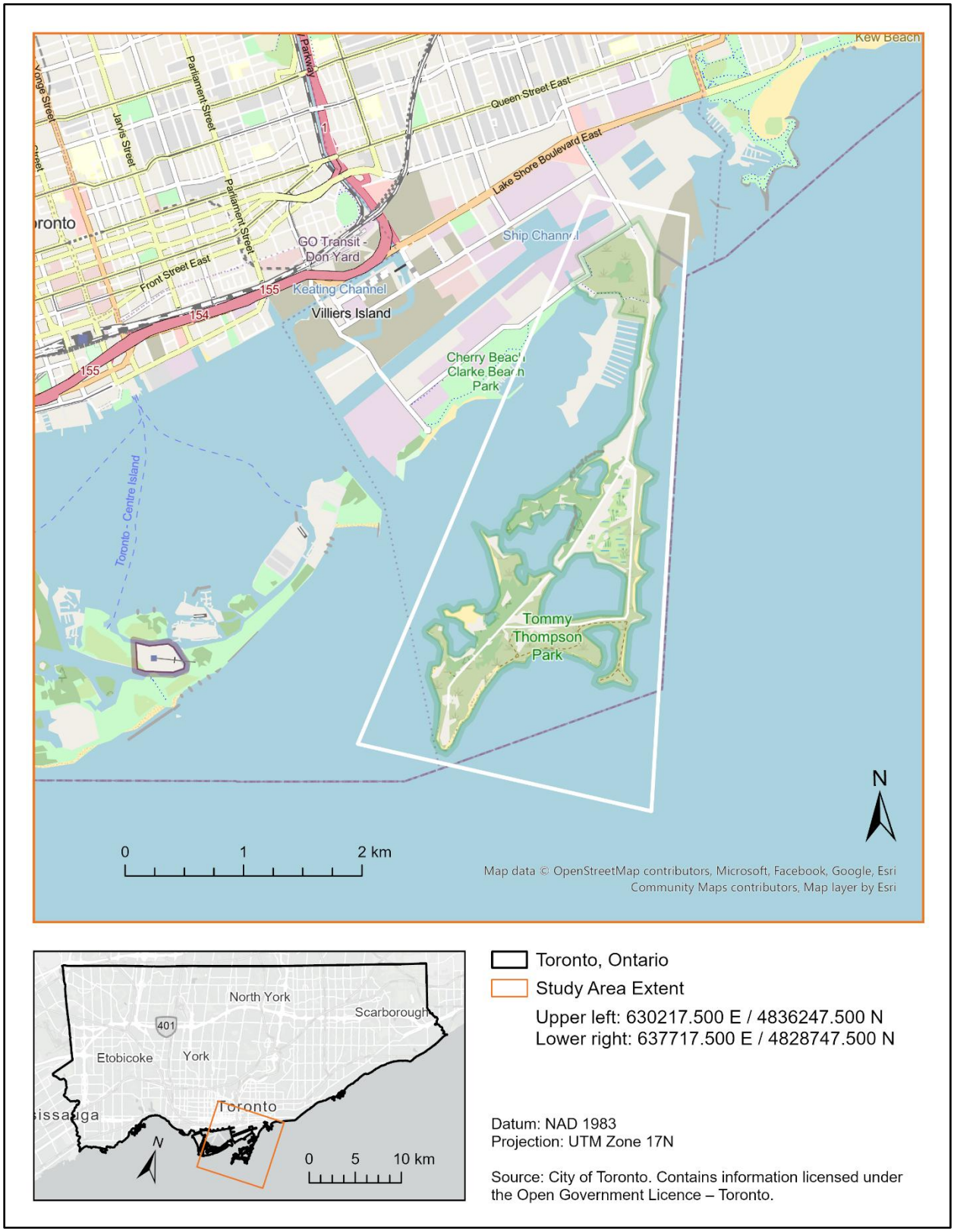

Figure 1: Map of the study area (the Leslie Street Spit) showing the full extent of the subset imagery and position within Toronto.

have formed by natural succession, and, since 1995, a "conservation by design" approach by the TRCA (Kehm, 2020; TRCA, 2020; TRCA, 2024). Through the innovative construction of landforms, drainage systems, orientation to prevailing winds, and seed sources from bird and mammal activity, the park's terrestrial and aquatic ecosystems have evolved from an engineered "spit"; this "urban wild" has been demonstrated as a design model of landscape resilience and diversity (Kehm, 2020). The park is now recognized as one of the best areas for greenspace improvement along the Toronto waterfront (TRCA, 2020).

1.3 Research Objectives

The objective of this research is to monitor vegetation expansion at the Leslie Street Spit over 50 years – the evolution of the Spit from a minimalist port-related facility to an "accidental wilderness" to an urban waterfront park will be observed and quantified. The rates of natural vegetation change (prior to 1995) and of natural and planned vegetation change resulting from habitat enhancement by the TRCA (from 1995 onward) will be compared. While the change detection methodology performed in this study cannot objectively distinguish natural succession from deliberate planting, the year 1995 will act as a key defining point that separates pure natural vegetation change from a combination of natural and planned change. Similar to a study from Ferrato and Forsythe (2013) involving a comparison of Landsat, Hyperion, and Satellite Pour L'Observation de la Terre (SPOT) data for the classification of the Lower Don River in Toronto, Ontario, the Spit's industrial beginnings make it a significant area for studying the quantity of vegetation cover. A secondary objective is to discover how leveraging various remote sensing algorithms can achieve the best possible classifications of the remotely sensed imagery, in order to aid the detection of vegetation change.

2. LITERATURE REVIEW AND METHODS

2.1 Data

Landsat data were obtained to observe the study area for the 1974 to 2024 period. Data obtained from Landsat missions have proven invaluable for conducting multitemporal analyses on vegetation expansion dynamics due to their suitable spectral, geometric, and temporal resolution (Mancino et al., 2025). The Landsat program is run by the United States Geological Survey (USGS) and is the longest-running source of remotely sensed data used for Earth observation (Forsythe and McCartney, 2014). A primary goal of this research was to perform a long-term analysis of the vegetation at Leslie Street Spit, reaching back as far as possible to the early stages of landform creation, so that important early natural succession could be captured. Other sensors were available, such as SPOT (launched in 1986), Advanced Spaceborne Thermal Emission and Reflection Radiometer (ASTER, launched in 1999), and Sentinel-2 (launched in 2015). These options have spatial resolutions similar to or better than Landsat sensors, but their data do not extend far enough into the past for the purposes of this research.

Landsat data are freely available at USGS EarthExplorer (USGS, 2026). A total of 12 Collection 2 Level-1 images forming nine image pairs were obtained from the platform. To help minimize seasonal vegetation differences and the effects of sun position variation, Sun et al. (2007) acquired images within the same approximate yearly timeframe for their urban sprawl land use classification study of Calgary, Alberta, using Landsat data. This approach is shared by Coppin and Bauer (1996), Forsythe (2004), Forsythe and Waters (2006), Forsythe et al. (2012), Alphan (2013), Forsythe and McCartney (2014), Mancino et al. (2014), and Mancino et al. (2025). This approach was utilized for this study, obtaining data acquired only within the month of July. Coppin and Bauer (1996) reviewed the methods and results of digital change detection with a case study of the northern United States forest ecosystem using Landsat data. They found that while visually

analyzing Landsat-1 Multispectral Scanner (MSS) data for forest cover regeneration assessment, a periodicity of at least five years was required to detect non-forest to forest changes, which would be applicable to the type of vegetation change studied at the Leslie Street Spit (Coppin and Bauer, 1996). Table 1 summarizes the imagery downloaded from USGS EarthExplorer (USGS, 2026).

Table 1: Data summary showing image acquisition dates with paths/rows, the capturing instrument, spatial resolution, and time interval between the image dates of each image pair (MSS = Multispectral Scanner, TM = Thematic Mapper, OLI = Operational Land Imager, WRS = World Reference System).

Landsat Instrument	Acquisition Date	Path / Row	Spatial Resolution (m)	Time Interval when Paired with Previous Image (years)
Landsat-1 MSS	1974-07-06	19 / 29 (WRS-1)	60	N/A
Landsat-2 MSS	1978-07-12	19 / 30 (WRS-1)	60	4
Landsat-4 MSS	1983-07-14	17 / 30 (WRS-2)	60	5
Landsat-5 TM	1984-07-24	17 / 30 (WRS-2)	30	N/A
Landsat-5 TM	1990-07-25	17 / 30 (WRS-2)	30	6
Landsat-5 TM	1995-07-14	18 / 30 (WRS-2)	30	5
Landsat-5 TM	2000-07-20	17 / 30 (WRS-2)	30	5
Landsat-5 TM	2005-07-25	18 / 30 (WRS-2)	30	5
Landsat-5 TM	2011-07-19	17 / 30 (WRS-2)	30	6
Landsat-8 OLI	2013-07-15	18 / 30 (WRS-2)	15 (pansharpened)	N/A
Landsat-8 OLI	2019-07-09	17 / 30 (WRS-2)	15 (pansharpened)	6
Landsat-9 OLI-2	2024-07-14	17 / 30 (WRS-2)	15 (pansharpened)	5

Hemati et al. (2021) conducted a review of the applications of Landsat data to change detection over 50 years and noted that with the availability of Collection 2 and other preprocessed products with automated cloud detection algorithms, there is now a robust capacity for using Landsat data in time series analysis and change detection applications. Collection 2 (released December 2020), similar to Collection 1, delivers surface reflectance data that are consistent in space and time as a physical property (Hemati et al., 2021). Collection 2 improves upon Collection 1 in terms of geometric accuracy, radiometric calibration, number of quality assessment bands, metadata quality, and features a cloud optimized file format (Hemati et al., 2021).

2.2 Pansharpening for Resolution Improvement and other Preprocessing Activities

Pansharpening involves improving the spatial resolution of a remotely sensed image using panchromatic data from the same or a different sensor. The methods used have not always provided

meaningful results – Landsat MSS and Thematic Mapper (TM) data were combined in the past with SPOT panchromatic data, which introduces the problem of land cover change occurring in the interim between the two sensors' acquisition dates when two different systems are used (Forsythe, 2004). Forsythe (2004) used pansharpened Landsat imagery to improve change detection classification in Toronto, Ontario and notes that same-sensor sharpening of Landsat data has been possible since the launch of Landsat-7 in 1999, with the addition of the 15 m panchromatic band. As emphasized by Forsythe and Waters (2006) – who explored the use of image texture measures for urban change detection in Calgary, Alberta using Landsat data – the PANSHARP algorithm, as implemented in the Catalyst Professional software (PCI Geomatics, 2026), eliminates problems such as destruction of data spectral characteristics, colour distortion, and operator and data set dependence, characteristic of some data fusion or sharpening processes. The PANSHARP results retain the multispectral variability of the original image (Forsythe, 2004). Pansharpening was employed in this study for the Landsat-8 Operational Land Imager (OLI) and Landsat-9 OLI-2 images.

Other preprocessing activities included visually ensuring that the study area portion of the images were free of clouds, visually investigating the images to ensure they were properly co-registered and aligned, merging the bands of each image together in Catalyst Professional into single PCIDSK (.pix) files (using the built-in Data Merge tool or manually using Translate and Transfer Layers utilities for Landsat MSS images), and repairing the file metadata. The file-level properties are not carried through during the data merge process, causing algorithms such as the Tasseled Cap Transformation to fail. Finally, the images were subset to the same geographic extent. Forsythe and McCartney (2014) found that subsetting the images decreases the overall file size considerably and increases the efficiency of the processing and classification algorithms, through

their investigation of forest disturbance in the Nagagamisis Central Plateau, Ontario using Landsat data. The entire footprint of the Leslie Street Spit was included in the extent of each image (Figure 1) as well as some surrounding features for context, such as the Toronto Islands, Woodbine Beach, Cherry Beach, Ashbridges Bay, and urban areas close to the waterfront. The geocoded extents are:

Upper left: 630217.500 E / 4836247.500 N
Lower right: 637717.500 E / 4828747.500 N

This achieved images of 500 pixels by 500 lines (Landsat OLI/OLI-2, 15 m resolution), 250 pixels by 250 lines (Landsat TM, 30 m resolution), and 125 pixels by 125 lines (Landsat MSS, 60 m resolution), covering an area of 56.25 square kilometres.

2.3 Image Band Differencing

Image band differencing is likely the most widely applied change detection algorithm and can be useful for a variety of geographic environments (Coppin and Bauer, 1996). It involves the subtraction of pixels between a pair of co-registered raster datasets in order to identify areas that have undergone change in that time period (Forsythe and McCartney, 2014). The USGS (2025) recommends the green (for peak vegetation/plant vigour), red (for discriminating vegetation slopes), or near-infrared (for biomass content and shorelines) bands for assessing vegetation. Alphan (2013) used image arithmetic and transformation methods for binary landscape change detection of the eastern Mediterranean coast of Türkiye using Landsat data and found that Band 3 (red) differencing yielded the highest classification accuracies among the visible and near-infrared band comparisons, and outperformed NDVI differencing as well. Lu et al. (2004), who explored the merits of different change detection approaches, also found visible red band data to be useful and accurate for change detection in vegetated and urban environments, but NDVI differencing yielded the best results for vegetation change detection. Coppin and Bauer (1996) found that the advantages of vegetation indices over single-band responses are their ability to considerably

reduce the data volume and to provide information not available in any single band. Masek et al. (2000), Pu et al. (2008), Mancino et al. (2014), Ezaidi et al. (2022), and Mancino et al. (2025) used NDVI layers for their image differencing operations, and this technique was selected to be applied to each image pair in this study. Since the VEGINDEX algorithm has no input parameter available for sensor specifications of Landsat-1 or -2 MSS, NDVI was computed for MSS images manually using Catalyst Professional's Raster Calculator.

The results of the differencing operations for image pairs that have undergone significant change appear very light or very dark (Forsythe and McCartney, 2014). Image differencing has been identified to outperform other change detection techniques, including post-classification ("delta") change detection in which images from two dates are classified, followed by pixel-based comparison between the classifications, which compounds classification errors and may lead to inaccurate results (Forsythe and McCartney, 2014). Pu et al. (2008) and Ataabadi et al. (2024) agree that the accuracy of change detection using classification of difference images is much higher than the accuracy of the post-classification comparison method. Lu et al. (2004) note, however, that image differencing can only provide change/non-change information, while post-classification comparison can provide a complete matrix of change directions (determination of which type of land cover changed to which dissimilar type). Image differencing was selected for this study.

2.4 Unsupervised Change Detection Classification

Pu et al. (2008) compared change detection methods for monitoring sparse vegetation coverage in Nevada, USA, using Compact Airborne Spectrographic Imager (CASI) imagery. They assert that the purpose of change detection is to extract the true land cover change areas while normalizing all other changes caused by other factors. To do this, Forsythe and McCartney (2014) used the Iterative Self-Organizing Data Analysis Techniques (ISODATA) unsupervised

classification algorithm to cluster the output band differencing raster datasets into three information classes ("regenerative change," "disturbance change," and "no change") based on the pixel values contained within the difference images. Ezaidi et al. (2022) found that unsupervised classification of the difference image is a useful technique to map and quantify objects and change from their study of anthropogenic vegetation cover degradation in the Arganeraie Biosphere Reserve, Morocco, using Landsat-derived NDVI. Unsupervised classification was chosen for this study over supervised approaches such as Random Forest because of the volume of classifications to perform (36) and it was the preferred method found through experimentation. Ataabadi et al. (2024) compared the performance of delta and image differencing change detection techniques in a case study of Kingston, Ontario, using high-resolution PlanetScope (PS2) imagery. They aggregated nine distinct classes into two categories of "changed" or "unchanged," yielding a binary change map. For this study, the K-means unsupervised classification algorithm with 20 classes and 20 iterations was selected (through experimentation) to further aggregate into "change" or "no change" classes. These quantities achieved the desired separation while minimizing unnecessary computational effort.

2.5 Computation of Additional Input Parameters

The aggregate unsupervised classifications of the difference images for each timestep (change detection classifications) were combined with a land cover unsupervised classification of the later date image in each pair in order to distinguish the type of change that occurred. Principal Components, the Tasseled Cap Transformation, NDVI, and/or Image Texture can be calculated as useful measures in addition to the original satellite bands for distinguishing land cover classes. By applying these image enhancement techniques, there is a greater possibility for class separability (Ferrato and Forsythe, 2013).

2.5.1 Principal Component Analysis

Principal Components (as implemented through the PCA algorithm in the Catalyst Professional software) can be valuable, as they provide a linear transformation that rotates the axes of image space along lines of maximum variance (Forsythe and Wheate, 2003). Each component (there can be as many components as there are input channels) highlights a different aspect or feature of the scene. The component that best points out the type of land cover being studied was selected as an additional input in classification. Through their investigation of avalanche slopes in Yoho National Park, British Columbia, using Landsat data, Forsythe and Wheate (2003) found that the major features not relevant to the study area are usually removed through the higher components. PCA is useful for outlining greenspace, as found by Ferrato and Forsythe (2013). Comber et al. (2016) applied a geographically weighted PCA (GWPCA) method to Moderate Resolution Imaging Spectroradiometer (MODIS) image data of the Tengarang region, Indonesia and found that adding GWPCA layers as inputs significantly improves land cover classification accuracy.

2.5.2 Tasseled Cap Transformation

The Tasseled Cap Transformation (as implemented through the TASSEL algorithm in Catalyst Professional) has been demonstrated to be effective for vegetation mapping and temporal land cover change detection (Cohen et al., 2002; Healey et al., 2005; Han et al., 2007; Forsythe and McCartney, 2014). Tasseled Cap reduces the six original Landsat reflectance bands to three components representative of physical land surface characteristics known as brightness, greenness, and wetness, accounting for most of the variance in an image scene and providing a reduction in data volume with minimal information loss (Forsythe and McCartney, 2014). Of particular interest is the greenness component, which contrasts the near-infrared and visible bands and highlights the

amount of green vegetation in the scene. Greenness is correlated with canopy closure, leaf area index, and fresh biomass, according to Crist and Cicone (1984), who built on the Tasseled Cap Transformation of Landsat MSS data – developed by Kauth and Thomas (1976) – to describe a new transformation of Landsat TM data.

2.5.3 Normalized Difference Vegetation Index

The Normalized Difference Vegetation Index (NDVI; as found in the VEGINDEX algorithm in Catalyst Professional) estimates the amount of green biomass in images (Forsythe and McCartney, 2014). It is an image ratio between the near-infrared (NIR) and red bands, based upon healthy vegetation and biomass absorption of red light for photosynthesis and reflection of NIR wavelengths (Masek et al., 2000; Mancino et al., 2014). Viana et al. (2019) performed land cover change detection of Beja, Portugal, using Landsat time-series data specified that NDVI is the most commonly used satellite-based measure to monitor vegetation due to its robust and simple interpretation. It considers the distinctive shape of the vegetation reflectance curve. Ferrato and Forsythe (2013) found that NDVI defines greenspace from urban areas, and separates vegetation from water bodies and roads. The ratio is defined as follows (Masek et al., 2000; USGS, 2025):

$$NDVI\ (MSS\ 1,2,3) = \frac{Band\ 7\ (NIR) - Band\ 5\ (Red)}{Band\ 7\ (NIR) + Band\ 5\ (Red)} \quad (1)$$

$$NDVI\ (MSS\ 4,5) = \frac{Band\ 4\ (NIR) - Band\ 2\ (Red)}{Band\ 4\ (NIR) + Band\ 2\ (Red)} \quad (2)$$

$$NDVI\ (TM) = \frac{Band\ 4\ (NIR) - Band\ 3\ (Red)}{Band\ 4\ (NIR) + Band\ 3\ (Red)} \quad (3)$$

$$NDVI\ (OLI) = \frac{Band\ 5\ (NIR) - Band\ 4\ (Red)}{Band\ 5\ (NIR) + Band\ 4\ (Red)} \quad (4)$$

2.5.4 Image Texture

Image Texture (as implemented through the TEX algorithm in Catalyst Professional) is computed from a set of connected pixels and measures the graininess of an image. Different texture bands can be combined with spectral data to increase classification accuracy, and different "window" sizes can be explored – Shaban and Dikshit (2001) tested windows varying in size from 3 × 3 to 13 × 13 pixels, and found that the best window size is 7 × 7 or 9 × 9. They observed improvements in classifying urban areas using texture measures from SPOT imagery in their study of Lucknow, India, and Assuit, Egypt. Through experimentation, a window size of 3 × 3 was found to be appropriate for this study. Forsythe and Waters (2006) found that of the many options that are available (including mean, dissimilarity, contrast, and homogeneity), mean texture measures delineate urban built-up areas well and distinguish urban and agricultural features, while dissimilarity details newly excavated areas well. Ferrato and Forsythe (2013) found that mean texture clearly defines urban areas from barren land, which may have similar spectral reflectance. Mean texture also effectively distinguishes tree canopy from water bodies (Ferrato and Forsythe, 2013). Berberoğlu et al. (2010) used image texture measures (the grey level co-occurrence matrix [GLCM – angular second moment, contrast, dissimilarity, and entropy] and variogram) to detect land cover change in wetlands on the southeastern Mediterranean Coast of Türkiye. They observed subtle spectral separation but distinct spatial patterns, such as small patches of semi-natural vegetation that formed a distinctive texture, thereby increasing change detection accuracy for sand dune vegetation and agriculture. For this study, dissimilarity achieved a desirable result.

2.6 Unsupervised Land Cover Classification

As previously mentioned, aggregate unsupervised classifications of land cover on the later date image in each pair (using the original Landsat image bands plus combinations of additional

input parameters) were combined with the change detection aggregate unsupervised classifications of the difference images. For these land cover classifications, the K-means unsupervised classification algorithm was once again employed – it is considered a robust classification method by Häme et al. (1998). Masek et al. (2000) studied urban growth dynamics in Washington, DC (USA) using Landsat data and found that 22 spectral clusters were sufficient to define classes of residential, commercial, agricultural, and forested land. A higher maximum number of clusters, such as 64 or 255, may result in greater class separability (Forsythe, 2004; Forsythe and Waters, 2006). An aggregation was completed by studying the original Landsat images visually to assign each spectral cluster to an information class (Forsythe and McCartney, 2014). In the case of the Leslie Street Spit, these classes consist of greenspace, water, and built land. The K-means unsupervised classification algorithm with 20 classes and 20 iterations was once again selected (through experimentation) to aggregate into the information classes. These quantities achieved adequate class separation while minimizing unnecessary computational effort. For each image pair, three possible classifications were assessed: original bands only, original bands plus one additional input parameter, and original bands plus two additional input parameters.

2.7 Accuracy Assessment

Post-classification accuracy assessments were employed to evaluate the quality of information derived from the land cover classifications. Forsythe and McCartney (2014) used a true colour composite as a reference image. A false-colour composite reference image was selected for this study because the main objective was vegetation identification. According to Congalton (1989), simple random and stratified random sampling provide satisfactory results. A wide variety of sampling approaches have been observed. Wilson and Sader (2002) generated a minimum of 495 points for each map in their evaluation of the effect of time intervals between image acquisition

dates on forest change accuracy using Landsat data. Zewdie and Csaplovies (2015) collected 450 stratified random samples in the field for ground-truthing and classification accuracy assessment in their Landsat study of land cover transformations of semi-arid regions in northwestern Ethiopia. Forsythe (2004) and Forsythe and McCartney (2014) used 300 random sample points, stratified proportionally to the number of pixels in each of the three information classes. Forsythe and Wheate (2003) and Forsythe et al. (2012) used 200 sample points while Forsythe and Waters (2006) used 150 points. Mancino et al. (2025) employed 90 control points randomly and proportionally selected from their study area, examined by visual analysis on orthophotos to verify forest recolonization. A total of 200 stratified random sample points were selected for each image pair in this study, using a reference image for visual analysis. This technique is a reliable method for accuracy assessment when ground truth data are not available (Wilson and Sader, 2002; Forsythe and McCartney, 2014). The decision to employ 200 sample points was based on the desire to achieve a middle ground between the various sample point quantities from other research, and to minimize unnecessary computational effort. Error (confusion) matrices and accuracy statistics were generated for each image classification, providing overall accuracy, producer's accuracy (a measure of omission error), and user's accuracy (a measure of commission error) (Congalton, 1989).

2.8 Quantifying Change via Raster Operations

For the final stage of the change detection procedure, Forsythe (2004) exported the image difference classification and best land cover classification rasters as Erdas Imagine (.img) files from Catalyst Professional to be analyzed in ArcGIS (Esri, 2026). For each timestep, the two classification results were exported to ArcGIS as GRID files and the change detection classification layer was reclassified. The two layers were combined using the addition operator of

the Raster Calculator (Spatial Analyst) tool (Forsythe, 2004). The result of this operation defines a change over the image pair's time interval in the land cover information classes. Since the chosen Landsat images cover a wider extent than the land occupied by the Leslie Street Spit, it was necessary to clip the overall change rasters to a more specific extent in ArcGIS Pro in order to identify the area of vegetation change on the Spit – a bounding polygon surrounding the Spit was created using the Extract By Mask (Spatial Analyst) tool to exclude the portions of the change rasters that lie outside the polygon. Forsythe and McCartney (2014) mapped the change for each time interval visually in ArcGIS and calculated total areas and annual rates of change. This can be done by multiplying the quantity of change pixels in the information class of interest (greenspace) by the size of each pixel (to achieve total area) and dividing by the size of the image pair's time interval (to achieve an annual rate). This technique was applied here, allowing comparison of rates of vegetation expansion prior to 1995 (natural vegetation change) and from 1995 onward (natural and planned vegetation change resulting from habitat enhancement) (TRCA, 2024).

3. RESULTS AND DISCUSSION

3.1 Image Classification and Accuracy Assessment

Combinations of input parameters for land cover classifications (to be assessed for best accuracy) were chosen as follows. Each image would have one option using the original bands only (MSS: Bands 4-7 / 1-4; TM: Bands 1-5, 7; OLI: Bands 2-7). A second option would involve the original bands plus one input parameter – they were selected such that all of the four input parameters were represented at least twice. The final option would involve the original bands plus the same input parameter from the second option, plus one other input parameter – the parameters were combined such that all of the permutations of two input parameters were represented at least once. Table 2 shows the results of the accuracy assessments. It shows that seven of the nine best classifications involved additional input parameters. Principal Components succeeded in one out of five sets (20%) in which it was included, Texture succeeded in two out of four (50%), NDVI succeeded in three out of four (75%), and Tasseled Cap succeeded in four out of five sets (80%).

The best land cover classification results are displayed in Figures 2 through 10. Three classes were employed: greenspace (green), water (blue), and built land (grey). It should be noted that even after increasing the number of spectral classes involved in classification significantly, little to no separation could be achieved between urban features and features such as the construction rubble beaches at the Leslie Street Spit – likely because the spectral signatures of intact buildings and concrete rubble are similar. Thus, “built” was applied to all areas in the scene that were not greenspace or water.

Table 2: Results of the land cover classification accuracy assessments. **Bold** indicates the most accurate classification of the three options. * Indicates a tie – the classification with fewer inputs was selected with which to proceed.

Image Date	Input Parameters	Overall Accuracy (%)	95% Confidence Interval (%)	Overall Kappa Statistic	Overall Kappa Variance
1978	Original bands only	87.500	(82.666 92.334)	0.745	-0.443
	Principal Component 2	87.500	(82.666 92.334)	0.749	-0.189
	PCA2 + Texture (Dissimilarity)	**88.000**	**(83.246 92.754)**	**0.757**	**-0.331**
1983	Original bands only	88.000	(83.246 92.754)	0.765	-0.153
	Texture (Dissimilarity)	**88.500**	**(83.829 93.171)**	**0.775**	**-0.143**
	Texture (Dissimilarity) + NDVI	85.000	(79.801 90.199)	0.712	-0.112
1990	Original bands only	85.500	(80.370 90.630)	0.711	-0.417
	Tasseled Cap Greenness*	**87.500**	**(82.666 92.334)**	**0.754**	**-0.174**
	Tasseled Cap Greenness + Texture (Dissimilarity)*	87.500	(82.666 92.334)	0.754	-0.174
1995	Original bands only	82.500	(76.984 88.016)	0.662	-0.131
	NDVI*	**83.500**	**(78.106 88.894)**	**0.681**	**-0.069**
	NDVI + Principal Component 5*	83.500	(78.106 88.894)	0.681	-0.069
2000	Original bands only	88.500	(83.829 93.171)	0.776	-0.090
	Tasseled Cap Greenness*	**89.000**	**(84.414 93.586)**	**0.786**	**-0.089**
	Tasseled Cap Greenness + Principal Component 4*	89.000	(84.414 93.586)	0.786	-0.089
2005	Original bands only	86.500	(81.514 91.486)	0.743	-0.049
	NDVI	84.000	(78.669 89.331)	0.687	-0.049
	NDVI + Tasseled Cap Greenness	**88.000**	**(83.246 92.754)**	**0.771**	**-0.021**
2011	**Original bands only***	**91.000**	**(86.784 95.216)**	**0.820**	**-0.238**
	Texture (Dissimilarity)*	91.000	(86.784 95.216)	0.820	-0.238
	Texture + Principal Component 4	90.500	(86.186 94.814)	0.811	-0.135
2019	Original bands only	93.000	(89.214 96.786)	0.860	-0.093
	Tasseled Cap Greenness	93.000	(89.214 96.786)	0.860	-0.093
	Tasseled Cap Greenness + NDVI	**95.000**	**(91.729 98.271)**	**0.900**	**-0.229**
2024	**Original bands only**	**91.000**	**(86.784 95.216)**	**0.826**	**-0.031**
	Principal Component 4	90.500	(86.186 94.814)	0.817	-0.035
	PCA4 + Tasseled Cap Greenness	90.000	(85.592 94.408)	0.807	-0.037

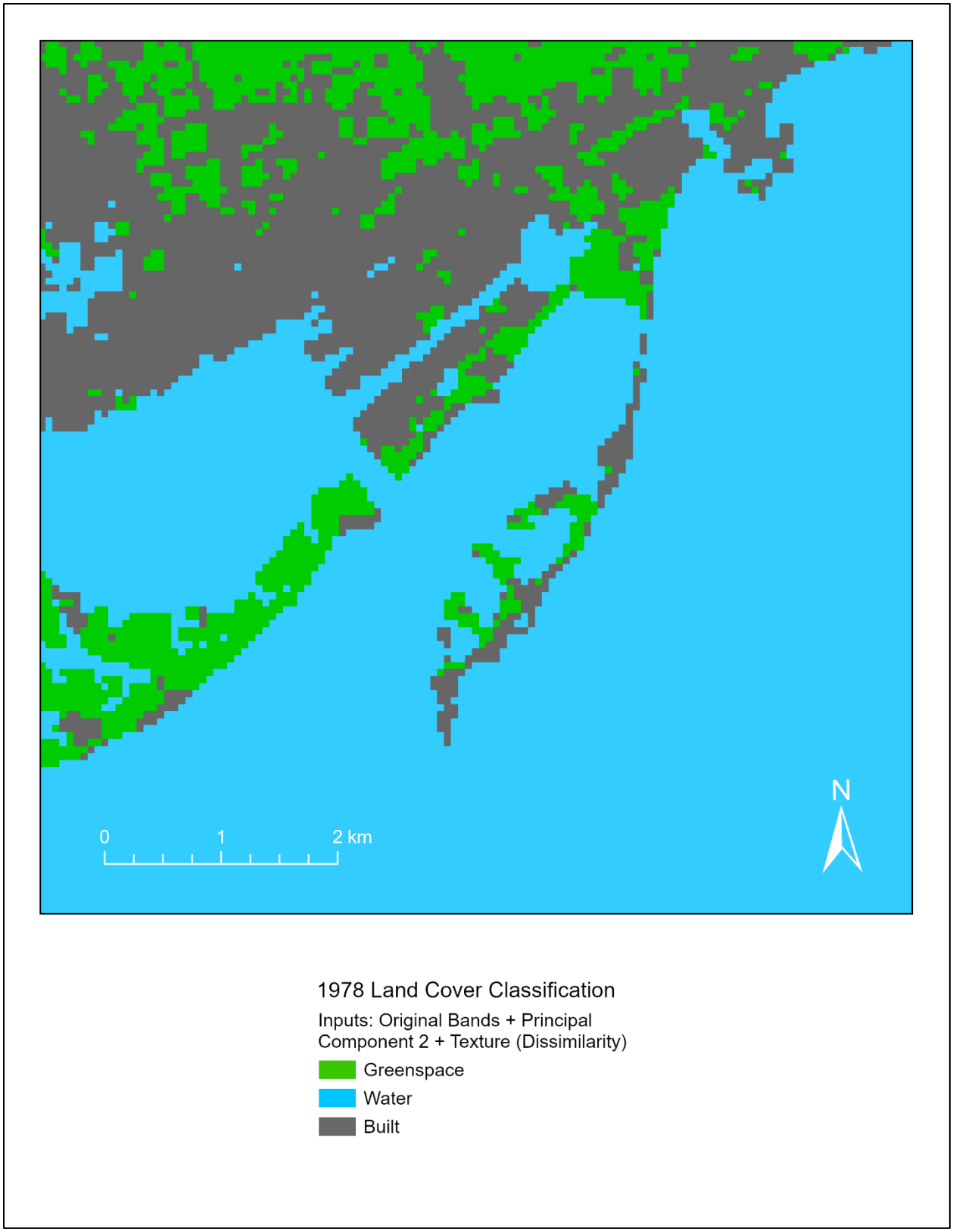

Figure 2: 1978-07-12 most accurate land cover classification. The input parameters were the original bands + Principal Component 2 + Texture (Dissimilarity).

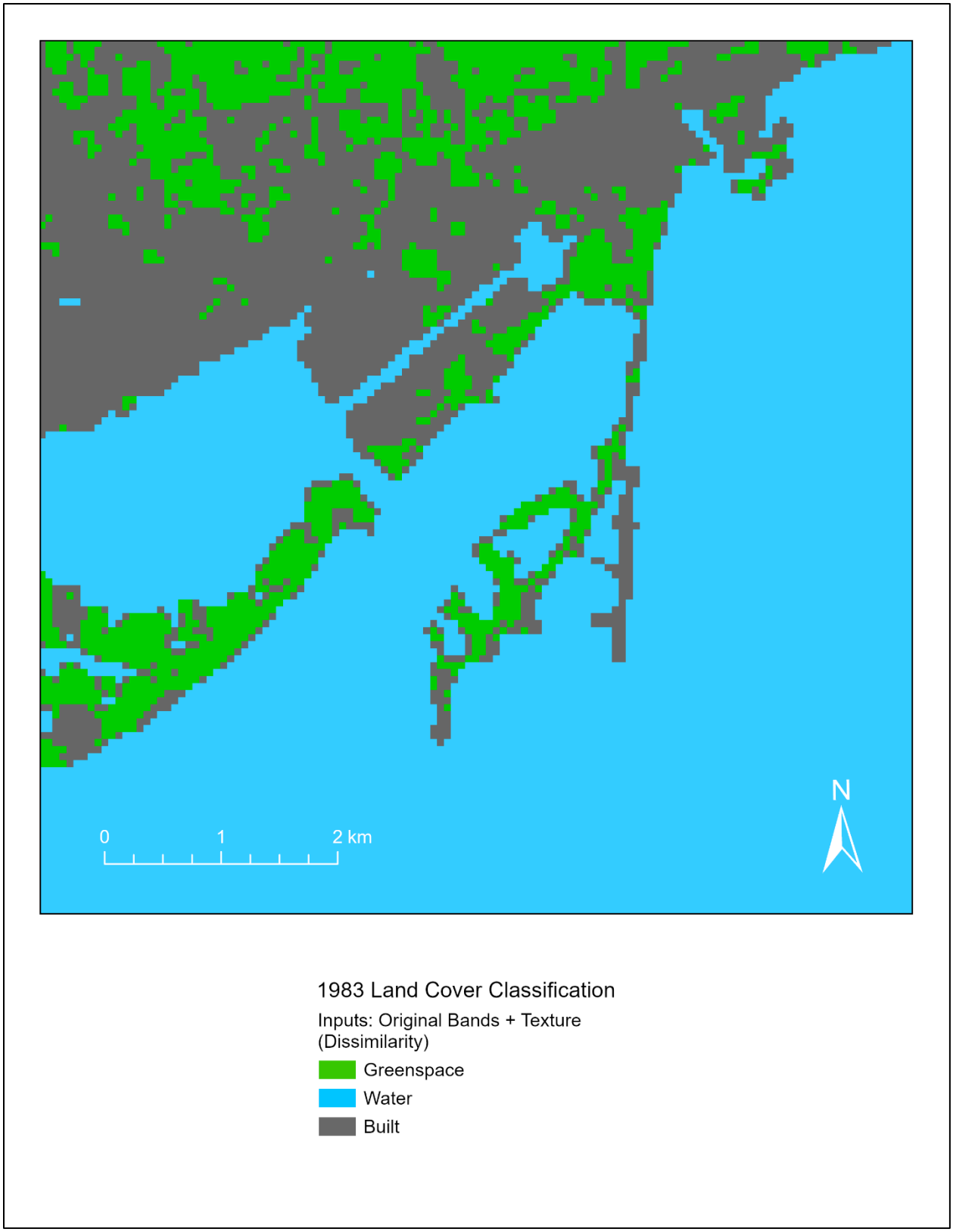

Figure 3: 1983-07-14 most accurate land cover classification. The input parameters were the original bands + Texture (Dissimilarity).

Tables 3 and 4 below present accuracy statistics and error matrices for the 1978 image (Figure 2). They indicate high accuracy in the water class, low producer's accuracy in the greenspace and built classes, and moderate confusion between greenspace and built land.

Table 3: 1978 accuracy report (best land cover classification result with input parameters of original bands + Principal Component 2 + Texture [Dissimilarity]).

Overall Accuracy: 88.000%			95% Confidence Interval: (83.246% 92.754%)		
Overall Kappa Statistic: 0.757			Overall Kappa Variance: -0.331		
Class	**Producer's Accuracy (%)**	**95% Confidence Interval (%)**	**User's Accuracy (%)**	**95% Confidence Interval (%)**	**Kappa Statistic**
Greenspace	68.000	(47.714 88.286)	73.913	(53.793 94.033)	0.7019
Water	98.462	(95.961 100.962)	92.754	(88.066 97.442)	0.7930
Built	68.889	(54.251 83.526)	79.487	(65.532 93.442)	0.7353

Table 4: 1978 error (confusion) matrix (best land cover classification result with input parameters of original bands + Principal Component 2 + Texture [Dissimilarity]).

Classified Data	**Reference Data**			
	Greenspace	Water	Built	Total
Greenspace	**18**	0	8	26
Water	2	**127**	7	236
Built	5	3	**30**	38
Total	25	130	45	200

Tables 5 and 6 below present accuracy statistics and error matrices for the 1983 image (Figure 3). They indicate high accuracy in the water class, low producer's accuracy in the greenspace class, and high confusion between greenspace and built land.

Table 5: 1983 accuracy report (best land cover classification result with input parameters of original bands + Texture [Dissimilarity]).

Overall Accuracy: 88.500%			95% Confidence Interval: (83.829% 93.171%)		
Overall Kappa Statistic: 0.775			Overall Kappa Variance: -0.143		
Class	**Producer's Accuracy (%)**	**95% Confidence Interval (%)**	**User's Accuracy (%)**	**95% Confidence Interval (%)**	**Kappa Statistic**
Greenspace	51.429	(33.442 69.415)	90.000	(74.352 105.648)	0.8788
Water	99.219	(97.303 101.135)	94.776	(90.636 98.917)	0.8549
Built	86.486	(74.119 98.854)	69.565	(55.181 83.949)	0.6266

Table 6: 1983 error (confusion) matrix (best land cover classification result with input parameters of original bands + Texture [Dissimilarity]).

Classified Data	**Reference Data**			
	Greenspace	Water	Built	Total
Greenspace	**18**	1	1	20
Water	3	**127**	4	134
Built	14	0	**32**	46
Total	35	128	37	200

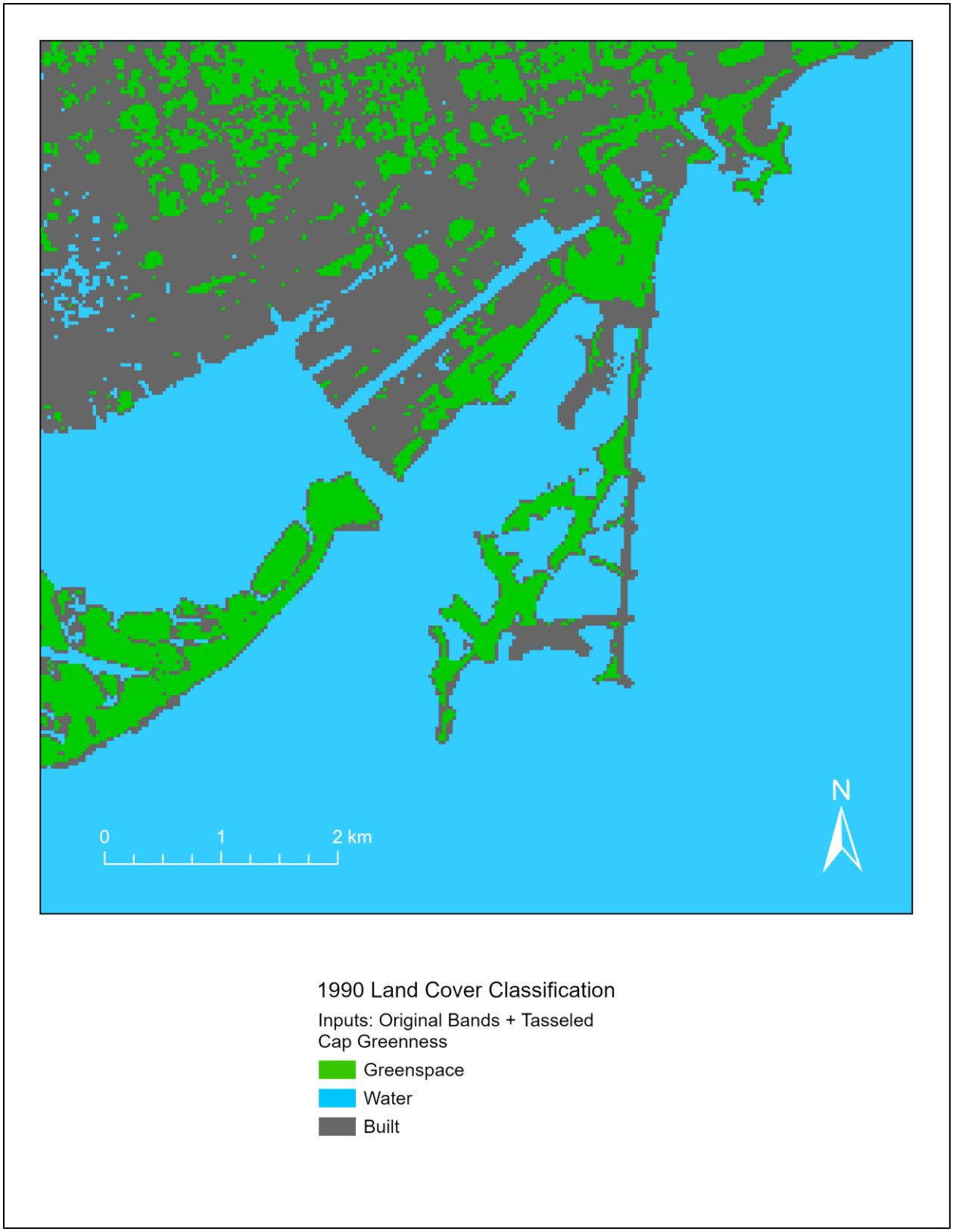

Figure 4: 1990-07-25 most accurate land cover classification. The input parameters were the original bands + Tasseled Cap Greenness.

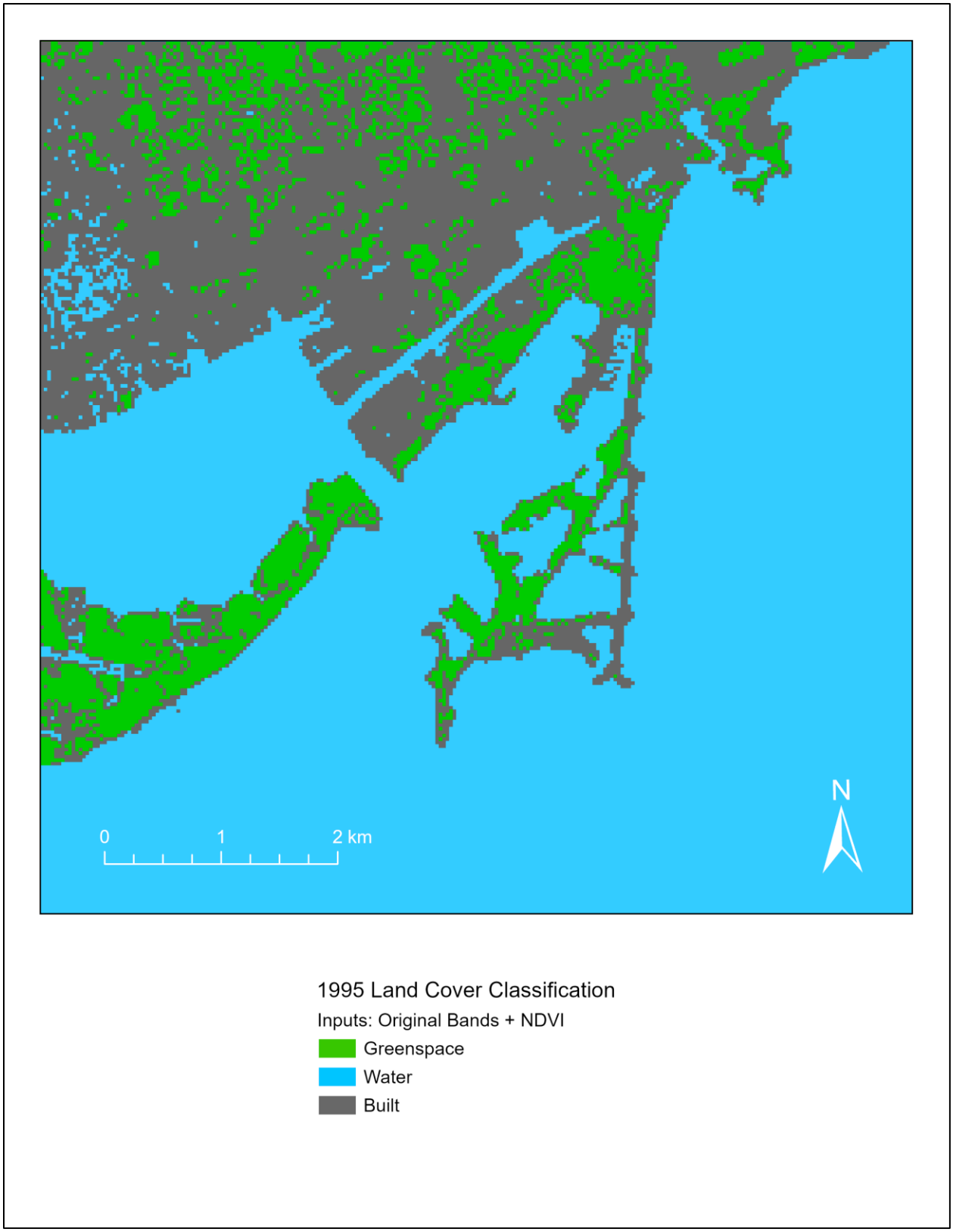

Figure 5: 1995-07-14 most accurate land cover classification. The input parameters were the original bands + NDVI.

Tables 7 and 8 below present accuracy statistics and error matrices for the 1990 image (Figure 4). They indicate high accuracy in the water class, low producer's accuracy in the greenspace class, and high confusion between greenspace and built land.

Table 7: 1990 accuracy report (best land cover classification result with input parameters of original bands + Tasseled Cap Greenness).

Overall Accuracy: 87.500%			95% Confidence Interval: (82.666% 92.334%)		
Overall Kappa Statistic: 0.754			Overall Kappa Variance: -0.174		
Class	**Producer's Accuracy (%)**	**95% Confidence Interval (%)**	**User's Accuracy (%)**	**95% Confidence Interval (%)**	**Kappa Statistic**
Greenspace	48.387	(29.182 67.592)	83.333	(63.339 103.328)	0.8028
Water	98.450	(95.930 100.969)	95.489	(91.585 99.392)	0.8729
Built	82.500	(69.475 95.525)	67.347	(53.196 81.498)	0.5918

Table 8: 1990 error (confusion) matrix (best land cover classification result with input parameters of original bands + Tasseled Cap Greenness).

Classified Data	**Reference Data**			
	Greenspace	Water	Built	Total
Greenspace	**15**	0	3	18
Water	2	**127**	4	133
Built	14	2	**33**	49
Total	31	129	40	200

Tables 9 and 10 below present accuracy statistics and error matrices for the 1995 image (Figure 5). They indicate high accuracy in the water class, low accuracy in the greenspace class, and high confusion between greenspace and built land.

Table 9: 1995 accuracy report (best land cover classification result with input parameters of original bands + NDVI).

Overall Accuracy: 83.500%			95% Confidence Interval: (78.106% 88.894%)		
Overall Kappa Statistic: 0.681			Overall Kappa Variance: -0.069		
Class	**Producer's Accuracy (%)**	**95% Confidence Interval (%)**	**User's Accuracy (%)**	**95% Confidence Interval (%)**	**Kappa Statistic**
Greenspace	45.161	(26.030 64.293)	63.636	(41.262 86.011)	0.5697
Water	93.182	(88.503 97.861)	96.850	(93.419 100.282)	0.9074
Built	81.081	(67.110 95.053)	58.824	(44.336 73.311)	0.4948

Table 10: 1995 error (confusion) matrix (best land cover classification result with input parameters of original bands + NDVI).

Classified Data	**Reference Data**			
	Greenspace	Water	Built	Total
Greenspace	**14**	5	3	22
Water	0	**123**	4	127
Built	17	4	**30**	51
Total	31	132	37	200

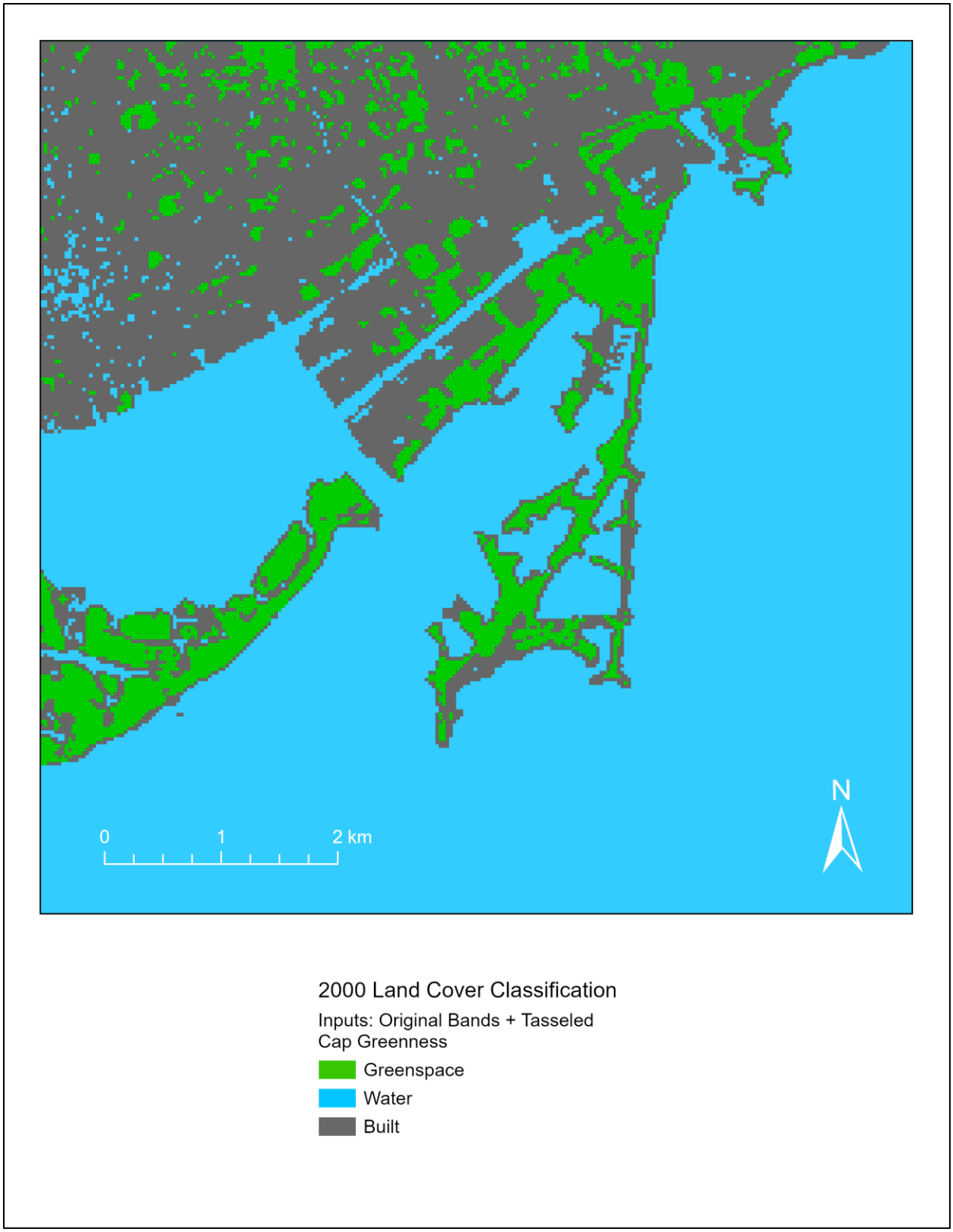

Figure 6: 2000-07-20 most accurate land cover classification. The input parameters were the original bands + Tasseled Cap Greenness.

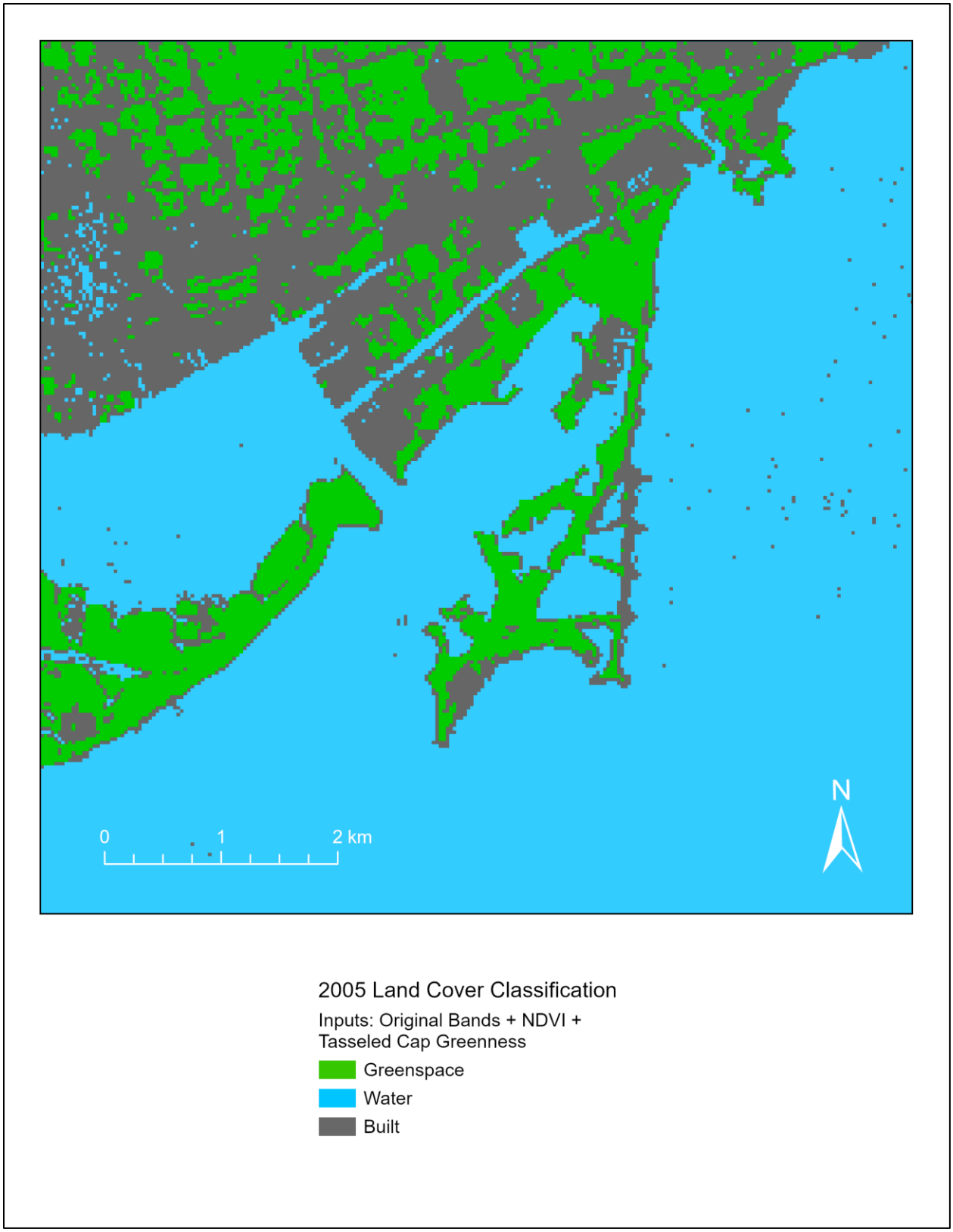

Figure 7: 2005-07-25 most accurate land cover classification. The input parameters were the original bands + NDVI + Tasseled Cap Greenness.

Tables 11 and 12 below present accuracy statistics and error matrices for the 2000 image (Figure 6). They indicate high accuracy in the water class, low producer's accuracy in the greenspace class, and high confusion between greenspace and built land.

Table 11: 2000 accuracy report (best land cover classification result with input parameters of original bands + Tasseled Cap Greenness).

Overall Accuracy: 89.000%			95% Confidence Interval: (84.414% 93.586%)		
Overall Kappa Statistic: 0.786			Overall Kappa Variance: -0.089		
Class	**Producer's Accuracy (%)**	**95% Confidence Interval (%)**	**User's Accuracy (%)**	**95% Confidence Interval (%)**	**Kappa Statistic**
Greenspace	53.571	(33.313 73.830)	83.333	(63.339 103.328)	0.8062
Water	95.420	(91.458 99.382)	98.425	(95.866 100.984)	0.9544
Built	92.683	(83.492 101.874)	69.091	(55.969 82.213)	0.6112

Table 12: 2000 error (confusion) matrix (best land cover classification result with input parameters of original bands + Tasseled Cap Greenness).

Classified Data	**Reference Data**			
	Greenspace	Water	Built	Total
Greenspace	**15**	2	1	18
Water	0	**125**	2	127
Built	13	4	**38**	55
Total	28	131	41	200

Tables 13 and 14 below present accuracy statistics and error matrices for the 2005 image (Figure 7). They indicate high accuracy in the water class, moderate accuracy in the greenspace and built classes, and moderate confusion between greenspace and built land.

Table 13: 2005 accuracy report (best land cover classification result with input parameters of original bands + NDVI + Tasseled Cap Greenness).

Overall Accuracy: 88.000%			95% Confidence Interval: (83.246% 92.754%)		
Overall Kappa Statistic: 0.771			Overall Kappa Variance: -0.021		
Class	**Producer's Accuracy (%)**	**95% Confidence Interval (%)**	**User's Accuracy (%)**	**95% Confidence Interval (%)**	**Kappa Statistic**
Greenspace	75.758	(59.621 91.895)	80.645	(65.124 96.166)	0.7682
Water	93.798	(89.249 98.348)	95.276	(91.192 99.359)	0.8669
Built	78.947	(64.669 93.226)	71.429	(56.575 86.282)	0.6473

Table 14: 2005 error (confusion) matrix (best land cover classification result with input parameters of original bands + NDVI + Tasseled Cap Greenness).

Classified Data	**Reference Data**			
	Greenspace	Water	Built	Total
Greenspace	**25**	2	4	31
Water	2	**121**	4	127
Built	6	6	**30**	42
Total	33	129	38	200

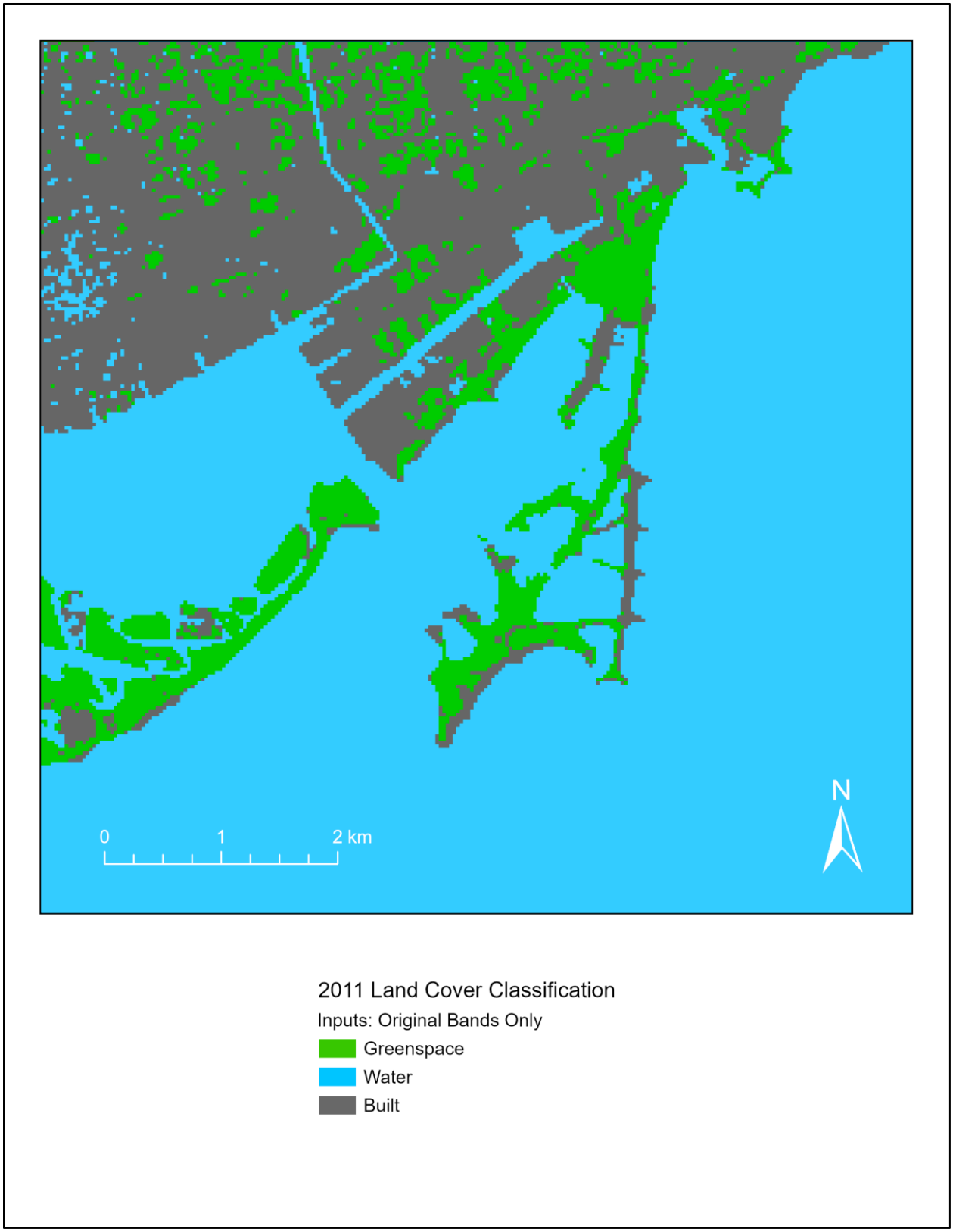

Figure 8: 2011-07-19 most accurate land cover classification. The input parameters were the original bands only.

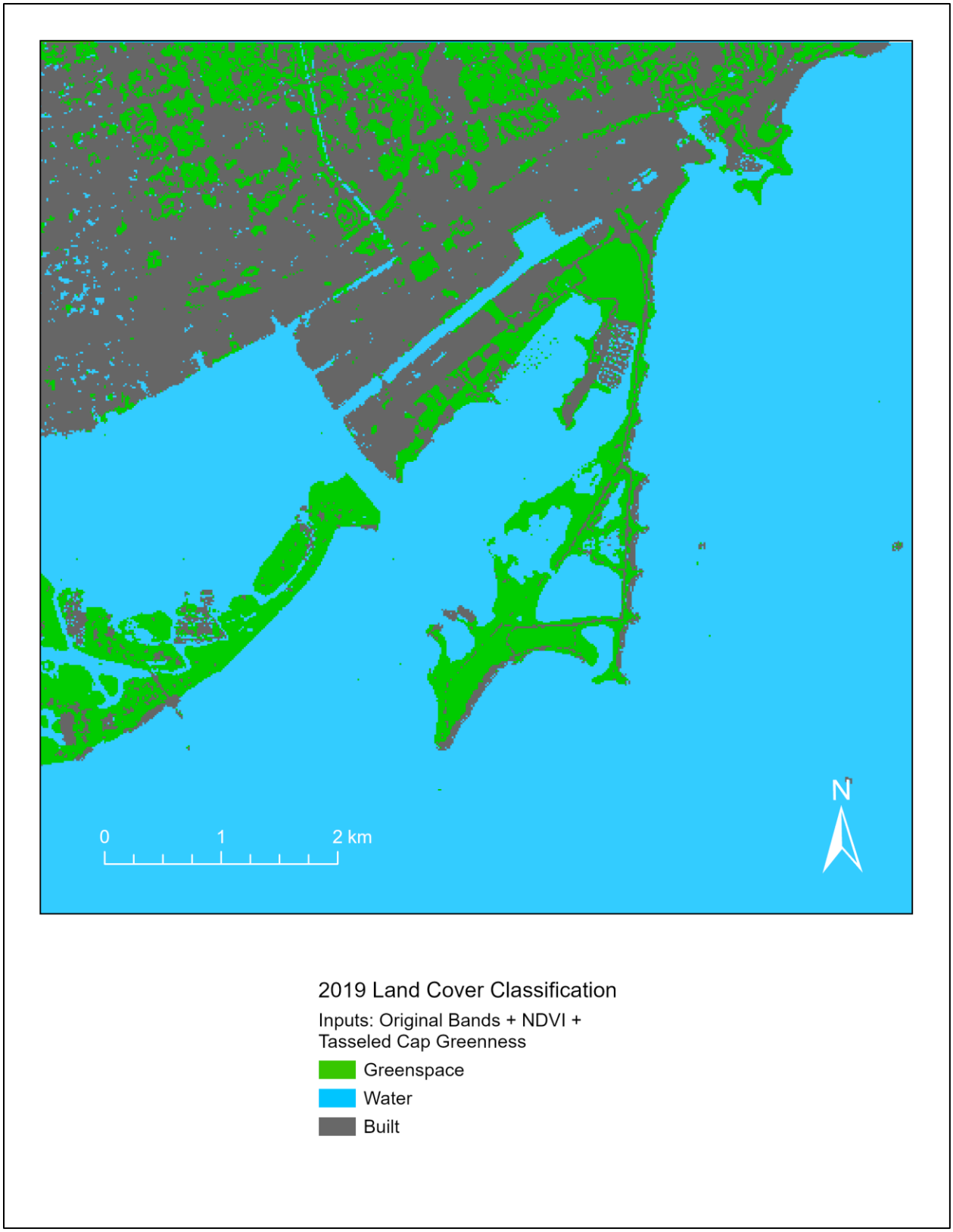

Figure 9: 2019-07-09 most accurate land cover classification. The input parameters were the original bands + NDVI + Tasseled Cap Greenness.

Tables 15 and 16 below present accuracy statistics and error matrices for the 2011 image (Figure 8). They indicate high accuracy in the water class, low producer's accuracy in the greenspace class, and moderate confusion between greenspace and built land.

Table 15: 2011 accuracy report (best land cover classification result with input parameters of original bands only).

Overall Accuracy: 91.000%			95% Confidence Interval: (86.784% 95.216%)		
Overall Kappa Statistic: 0.820			Overall Kappa Variance: -0.238		
Class	**Producer's Accuracy (%)**	**95% Confidence Interval (%)**	**User's Accuracy (%)**	**95% Confidence Interval (%)**	**Kappa Statistic**
Greenspace	66.667	(44.123 89.210)	73.684	(51.252 96.116)	0.7060
Water	96.947	(93.619 100.275)	96.212	(92.577 99.848)	0.8902
Built	85.417	(74.390 96.443)	83.673	(72.304 95.043)	0.7852

Table 16: 2011 error (confusion) matrix (best land cover classification result with input parameters of original bands only).

Classified Data	**Reference Data**			
	Greenspace	Water	Built	Total
Greenspace	**14**	3	2	19
Water	0	**127**	5	132
Built	7	1	**41**	49
Total	21	131	48	200

Tables 17 and 18 below present accuracy statistics and error matrices for the 2019 image (Figure 9). They indicate high accuracy in the water class, high accuracy in the greenspace and built classes, and low confusion between greenspace and built land.

Table 17: 2019 accuracy report (best land cover classification result with input parameters of original bands + NDVI + Tasseled Cap Greenness).

Overall Accuracy: 95.000%			95% Confidence Interval: (91.729% 98.271%)		
Overall Kappa Statistic: 0.900			Overall Kappa Variance: -0.229		
Class	**Producer's Accuracy (%)**	**95% Confidence Interval (%)**	**User's Accuracy (%)**	**95% Confidence Interval (%)**	**Kappa Statistic**
Greenspace	86.957	(71.019 102.894)	80.000	(62.320 97.680)	0.7740
Water	96.992	(93.714 100.271)	98.473	(95.992 100.955)	0.9544
Built	93.182	(84.598 101.766)	93.182	(84.598 101.766)	0.9126

Table 18: 2019 error (confusion) matrix (best land cover classification result with input parameters of original bands + NDVI + Tasseled Cap Greenness).

Classified Data	**Reference Data**			
	Greenspace	Water	Built	Total
Greenspace	**20**	3	2	25
Water	1	**129**	1	131
Built	2	1	**41**	44
Total	23	133	44	200

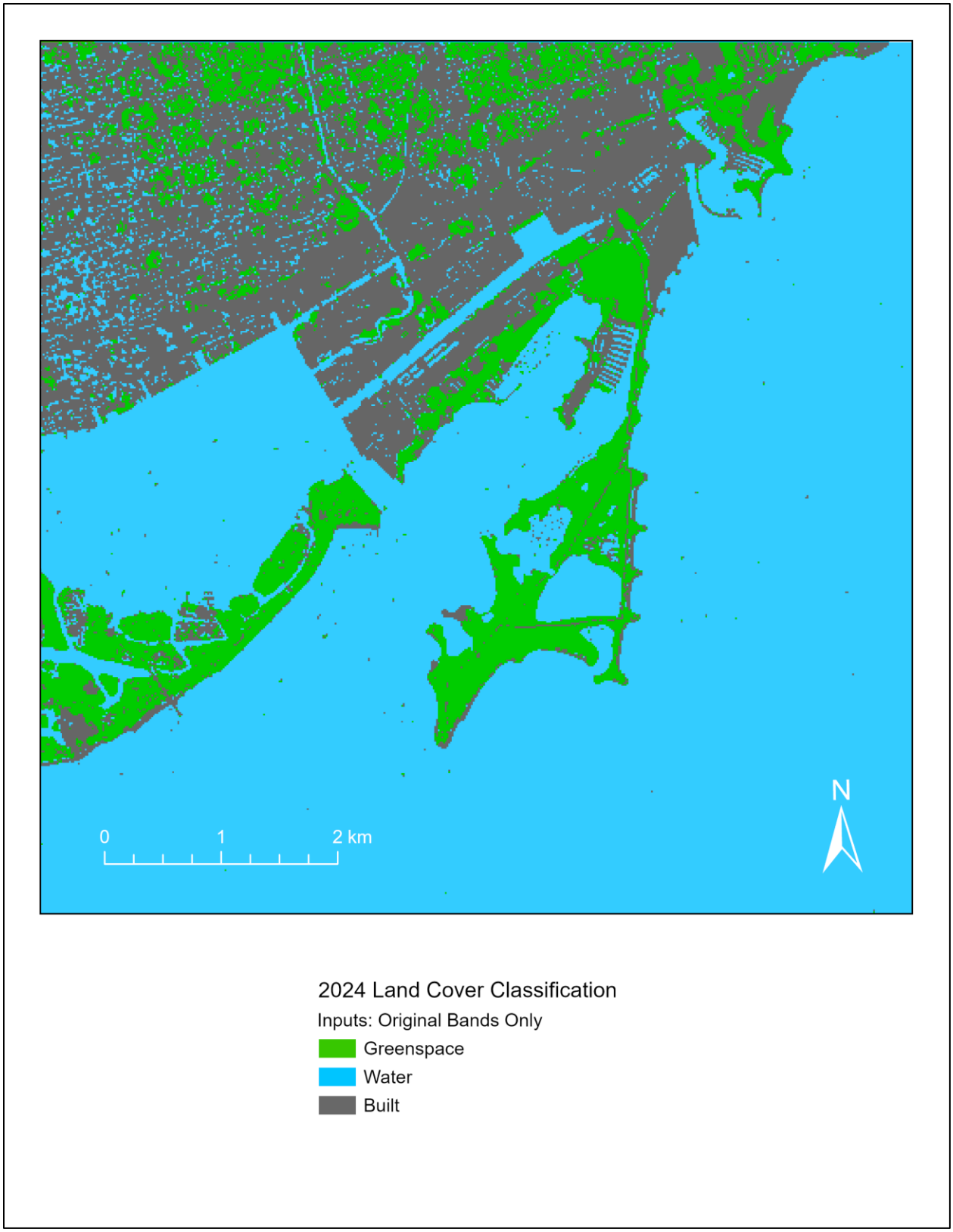

Figure 10: 2024-07-14 most accurate land cover classification. The input parameters were the original bands only.

Tables 19 and 20 below present accuracy statistics and error matrices for the 2024 image (Figure 10). They indicate high accuracy in the water class, moderate accuracy in the greenspace class, and low confusion between greenspace and built land.

Table 19: 2024 accuracy report (best land cover classification result with input parameters of original bands only).

Overall Accuracy: 91.000%			95% Confidence Interval: (86.784% 95.216%)		
Overall Kappa Statistic: 0.826			Overall Kappa Variance: -0.031		
Class	**Producer's Accuracy (%)**	**95% Confidence Interval (%)**	**User's Accuracy (%)**	**95% Confidence Interval (%)**	**Kappa Statistic**
Greenspace	79.167	(60.835 97.498)	79.167	(60.835 97.498)	0.7633
Water	97.619	(94.560 100.678)	94.615	(90.351 98.880)	0.8545
Built	80.000	(67.913 92.087)	86.957	(76.137 97.776)	0.8261

Table 20: 2024 error (confusion) matrix (best land cover classification result with input parameters of original bands only).

Classified Data	**Reference Data**			
	Greenspace	Water	Built	Total
Greenspace	**19**	1	4	24
Water	1	**123**	6	130
Built	4	2	**40**	46
Total	24	126	50	200

Accuracy results in the greenspace class are quite variable due to the small proportion of greenspace pixels in each image relative to the other two classes. The MSS images had producer's accuracies of 68.0% (1978 – inputs of original bands + Principal Component 2 + Texture [Dissimilarity]) and 51.4% (1983 – inputs of original bands + Texture [Dissimilarity]), meaning that the classifier omitted a considerable quantity of pixels that were found to be greenspace on the reference image. Conversely, the MSS images had user's accuracies of 73.9% (1978) and 90.0% (1983), meaning that the classifier mislabeled a relatively small quantity of pixels as greenspace that were found to be water or built land on the reference image. Kappa statistics (indicating, between 0 and 1, how much the classifications improve upon random guessing) were 0.7019 (1978) and 0.8788 (1983). The five TM images had producer's accuracies ranging between 45.2% (1995 – inputs of original bands + NDVI) and 75.8% (2005 – inputs of original bands + NDVI + Tasseled Cap Greenness), meaning that the classifier varied between omitting a moderately high quantity

of greenspace pixels to a relatively small quantity. User's accuracies were generally superior, ranging between 63.6% (1995) and 83.3% (1990 and 2000 – both with inputs of original bands + Tasseled Cap Greenness), meaning that the classifier varied between mislabeling a moderate quantity of pixels as greenspace to a relatively small quantity. Kappa statistics ranged between 0.5697 (1995) and 0.8062 (2000). Finally, the OLI images had producer's accuracies of 87.0% (2019 – inputs of original bands + NDVI + Tasseled Cap Greenness) and 79.2% (2024 – inputs of original bands only), certainly the best greenspace producer's accuracies of the nine images. This indicates that the classifier omitted a small quantity of pixels that were found to be greenspace on the reference image. User's accuracies were 80.0% (2019) and 79.2% (2024), meaning that the classifier mislabeled a relatively small quantity of pixels as greenspace that were found to be water or built land on the reference image. Kappa statistics were 0.7740 (2019) and 0.7633 (2024).

3.2 Vegetation Expansion Mapping

Change detection mapping of vegetation on the Leslie Street Spit involved the arithmetic addition of the land cover classification results from Section 3.1 and the NDVI difference change detection classification for each time period. Figure 11 provides a map showing the areas of the Spit referred to in this section. In Figures 12 through 20, coloured areas represent vegetation change for the current timestep and grey areas represent change that occurred prior to that timestep. False colour composites are shown underneath Figures 12 and 13 for context (true colour composites are not possible for MSS) and true colour composites underlay Figures 14 through 20. A simplified white bounding polygon illustrates the specific study area extent of the Leslie Street Spit, but a more refined polygon (not pictured) was used to clip the overall change rasters covering the entire scene to the desired extent.

Figure 11: Map of the study area (the Leslie Street Spit) zoomed to show more detailed features of the landform.

1974 to 1978

Figure 12 shows vegetation expansion due to natural succession on the newly formed peninsulas on the west side of the spine road. There is also some expansion on the Baselands. In the four-year period between 1974 and 1978, the present vegetation expansion class reveals 39.6 ha (396,000 m^2) of growth or an average annual expansion of 9.90 ha/year (99,000 m^2/year), the highest annual growth of any timestep.

1978 to 1983

Figure 13 shows vegetation expansion due to natural succession continuing on the peninsulas on the west side of the spine road, and on the spine road itself. A new peninsula to the east has been built (the Endikement), but has not seen any vegetation growth. In the five-year period between 1978 and 1983, the present vegetation expansion class reveals 26.6 ha (266,400 m^2) of growth or an average annual expansion of 5.33 ha/year (53,280 m^2/year).

1984 to 1990

Figure 14 shows vegetation expansion on the newly built marina, the Baselands, the Endikement Tip, and other various small areas. A large new construction (the Flats) connects the western peninsulas and Endikement and has not seen any vegetation growth thus far. In the six-year period between 1984 and 1990, the present vegetation expansion class reveals 10.4 ha (103,500 m^2) of growth or an average annual expansion of 1.73 ha/year (17,250 m^2/year).

1990 to 1995

Figure 15 shows vegetation expansion on the marina and the beginning of some natural succession on the Flats. In the five-year period between 1990 and 1995, the present vegetation expansion class reveals 8.19 ha (81,900 m^2) of growth or an average annual expansion of 1.64 ha/year (16,380 m^2/year).

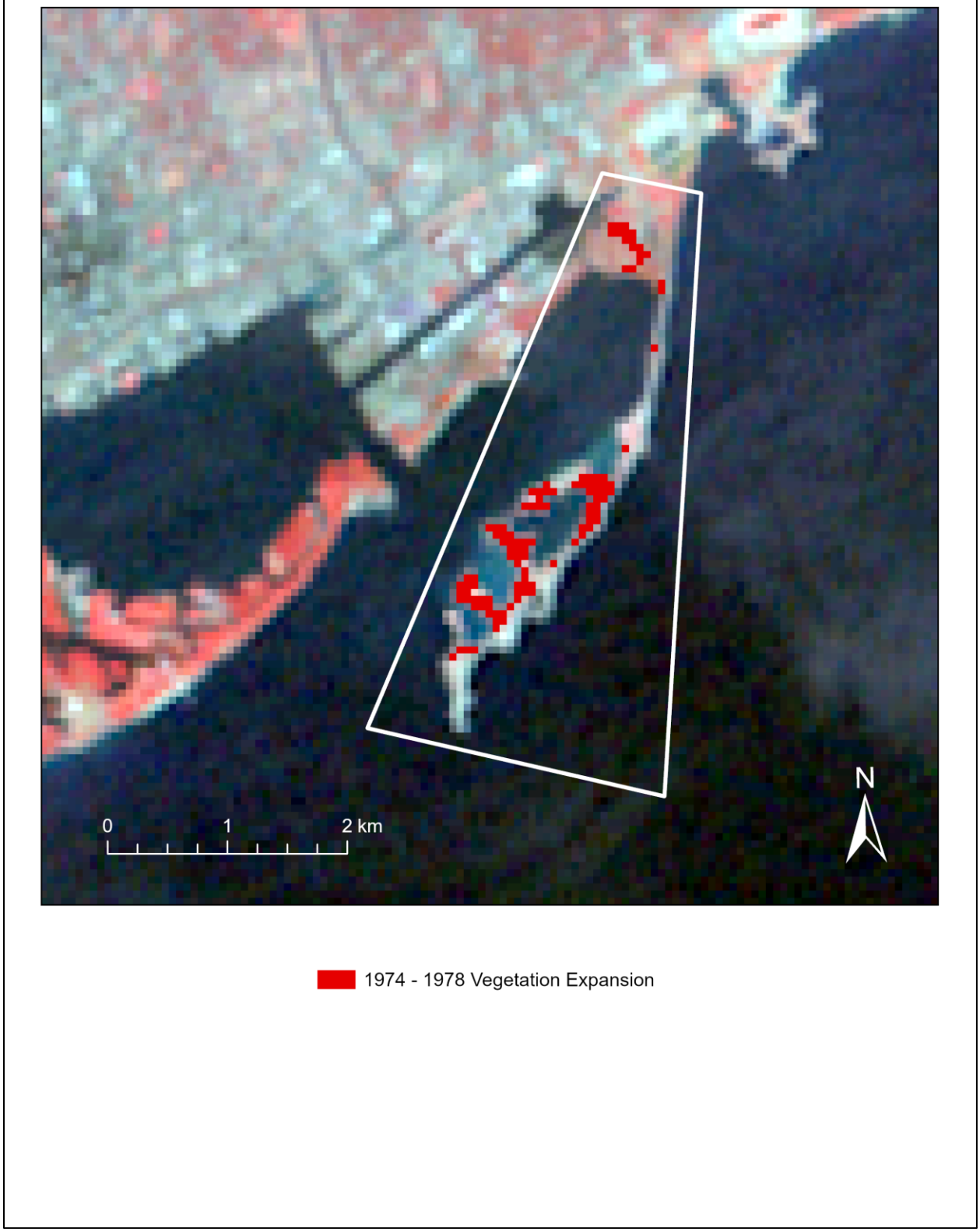

Figure 12: 1974 to 1978 vegetation expansion on the specific study area extent with 1978 false colour composite.

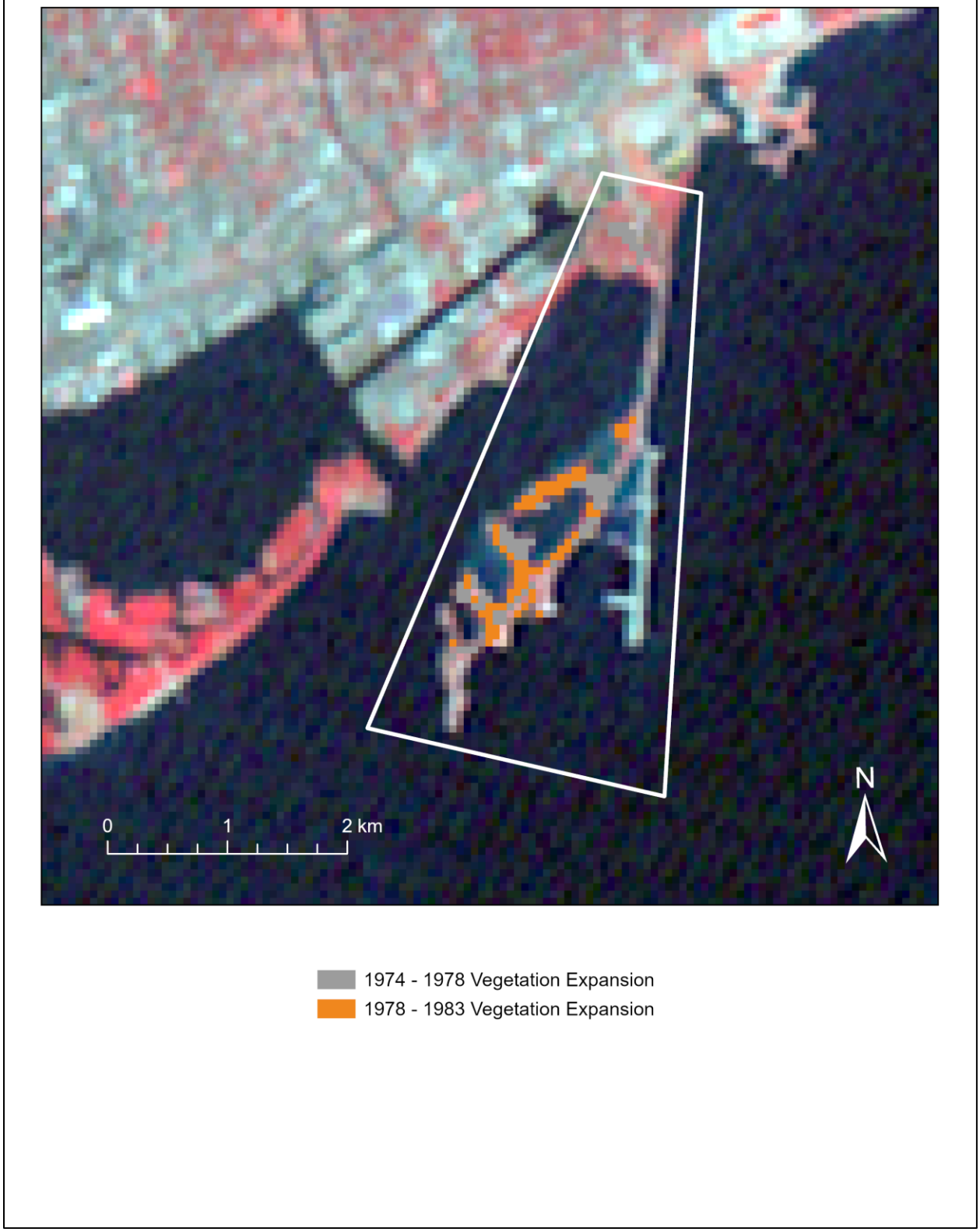

Figure 13: 1978 to 1983 vegetation expansion on the specific study area extent and past expansion, with 1983 false colour composite.

Figure 14: 1984 to 1990 vegetation expansion on the specific study area extent and past expansion, with 1990 true colour composite.

Figure 15: 1990 to 1995 vegetation expansion on the specific study area extent and past expansion, with 1995 true colour composite.

1995 to 2000

Figure 16 shows vegetation expansion on the marina, the Baselands, the spine road, the Endikement, and the Flats. The Toplands have begun to take shape, connecting the Flats to Lighthouse Point. In the five-year period between 1995 and 2000, the present vegetation expansion class reveals 29.5 ha (295,200 m^2) of growth or an average annual expansion of 5.90 ha/year (59,040 m^2/year).

2000 to 2005

Figure 17 shows vegetation expansion on the Baselands and various other small areas. The Toplands have continued their construction. In the five-year period between 2000 and 2005, the present vegetation expansion class reveals 4.86 ha (48,600 m^2) of growth or an average annual expansion of 0.972 ha/year (9,720 m^2/year), the least total or annual growth of any timestep.

2005 to 2011

Figure 18 shows vegetation expansion on the Baselands, spine road, Endikement Tip, the Flats, and the Toplands. In the six-year period between 2005 and 2011, the present vegetation expansion class reveals 49.3 ha (493,200 m^2) of growth (the most total growth of any timestep) or an average annual expansion of 8.22 ha/year (82,200 m^2/year).

2013 to 2019

Figure 19 shows vegetation expansion on the marina, Embayment D, Cell 2, the Endikement, the coast of the Flats, and the western peninsulas. In the six-year period between 2013 and 2019, the present vegetation expansion class reveals 22.4 ha (223,875 m^2) of growth or an average annual expansion of 3.73 ha/year (37,313 m^2/year).

Figure 16: 1995 to 2000 vegetation expansion on the specific study area extent and past expansion, with 2000 true colour composite.

Figure 17: 2000 to 2005 vegetation expansion on the specific study area extent and past expansion, with 2005 true colour composite.

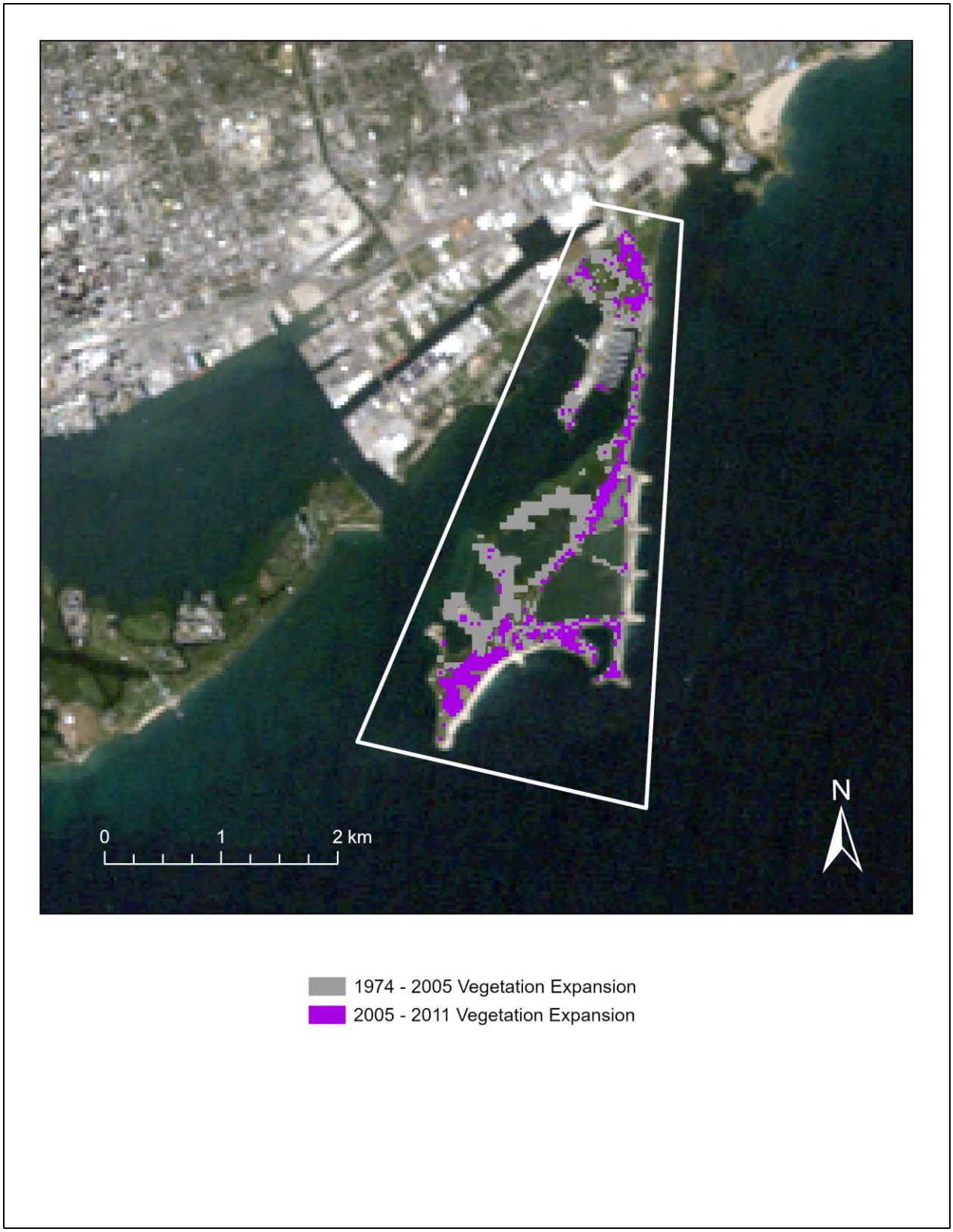

Figure 18: 2005 to 2011 vegetation expansion on the specific study area extent and past expansion, with 2011 true colour composite.

Figure 19: 2013 to 2019 vegetation expansion on the specific study area extent and past expansion, with 2019 true colour composite.

Figure 20: 2019 to 2024 vegetation expansion on the specific study area extent and past expansion, with 2024 true colour composite.

2019 to 2024

Figure 20 shows vegetation expansion on Embayment D, Cell 1, and the western peninsulas. In the five-year period between 2019 and 2024, the present vegetation expansion class reveals 22.0 ha (220,050 m^2) of growth or an average annual expansion of 4.40 ha/year (44,010 m^2/year).

Table 21 and Figure 21 summarize the results. The 1974 to 1978 period experienced the most average annual vegetation expansion, due to natural succession following intense landform expansion. In the 1974 to 1995 period (a 21-year time interval) – a period defined by natural growth – approximately 84.8 ha (847,800 m^2) of vegetation expansion occurred, at an average annual rate of 4.04 ha/year. Subsequently, in the 1995 to 2024 period (a 29-year time interval) – a period defined by natural and planned vegetation growth via habitat enhancement by the TRCA – approximately 128 ha (1,280,925 m^2) of vegetation expansion occurred, at an average annual rate of 4.42 ha/year. These rates are comparable, but the 1995 to 2024 period saw an increased rate of vegetation expansion. The total area of vegetation expansion over 50 years is estimated at 213 ha (2,128,725 m^2), with an average annual rate of 4.26 ha/year. Figure 22 shows all change rasters displayed cumulatively on a single map.

Table 21: Summary of vegetation expansion for each time period, with total and annual expansion.

Time Interval	Greenspace Expansion Pixel Quantity	Pixel Area (m^2)	Total Greenspace Expansion Area (ha)	Time Interval (years)	Average Annual Greenspace Expansion Area (ha/year)
1974 – 1978	110	3,600	39.6	4	9.90
1978 – 1983	74	3,600	26.6	5	5.33
1984 – 1990	115	900	10.4	6	1.73
1990 – 1995	91	900	8.19	5	1.64
1995 – 2000	328	900	29.5	5	5.90
2000 – 2005	54	900	4.86	5	0.972
2005 – 2011	548	900	49.3	6	8.22
2013 – 2019	995	225	22.4	6	3.73
2019 – 2024	978	225	22.0	5	4.40

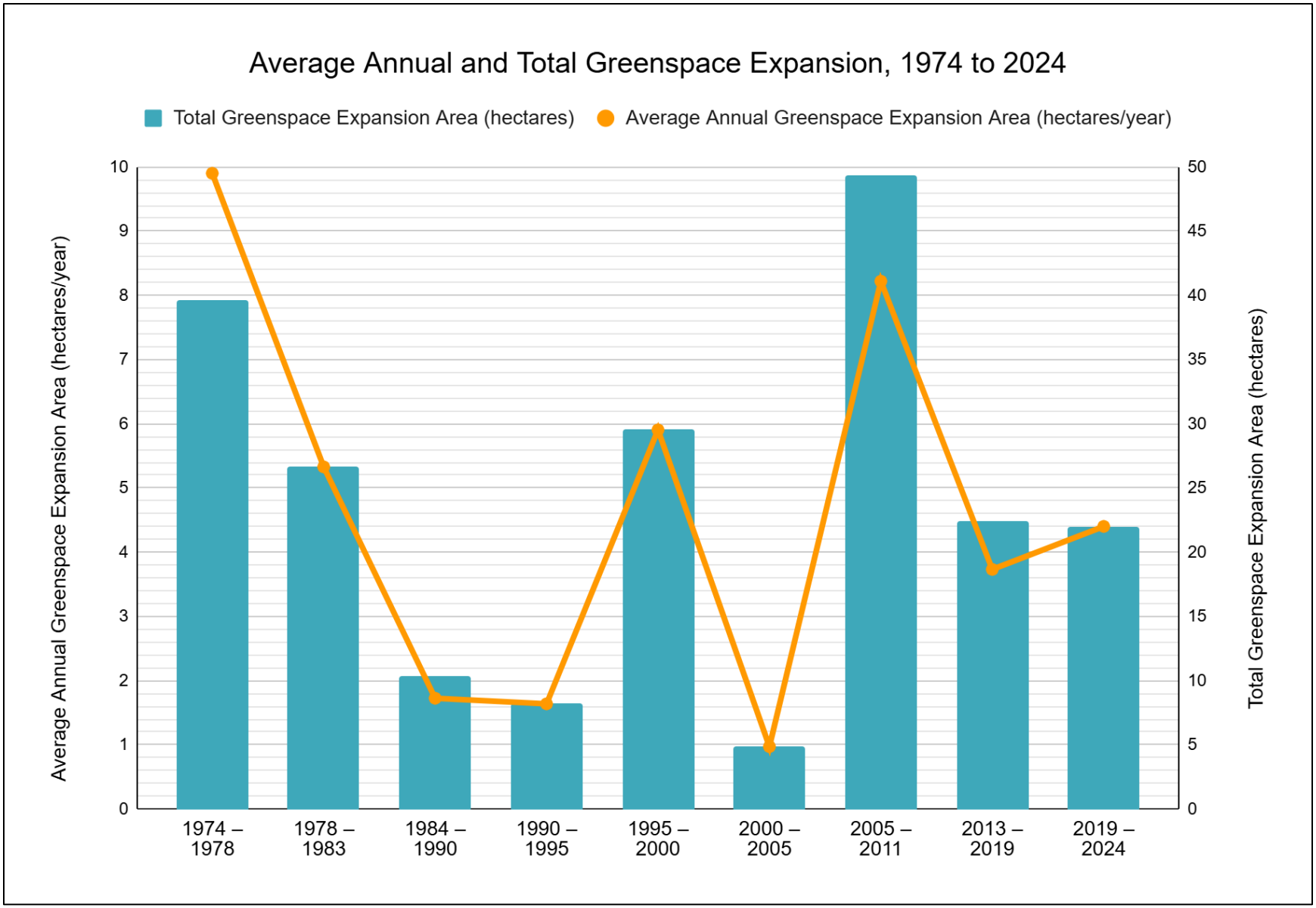

Figure 21: Chart showing average annual and total vegetation expansion over the study period.

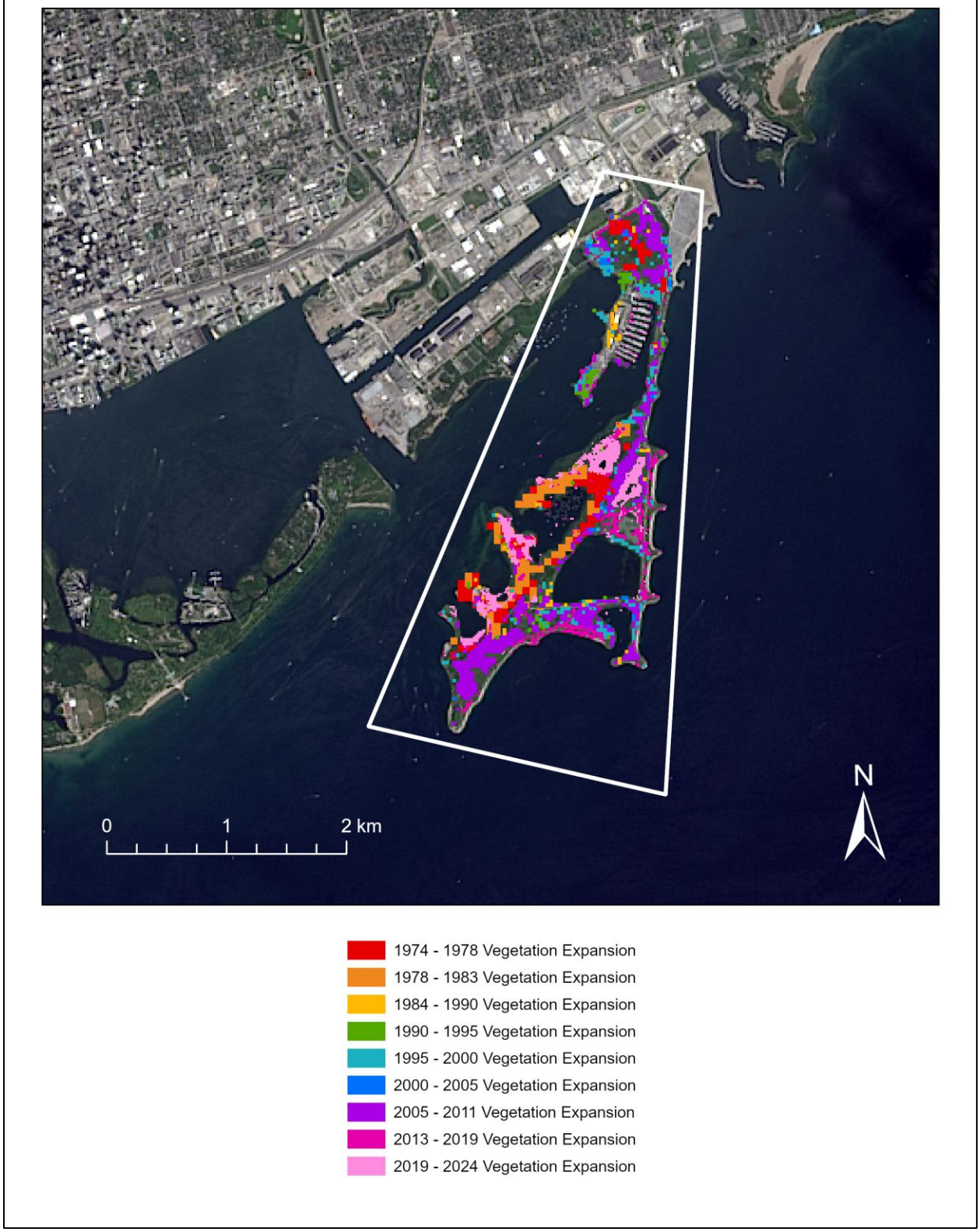

Figure 22: 1974 to 2024 cumulative vegetation expansion on the specific study area extent, with 2024 true colour composite.

4. CONCLUSION

The data and remote sensing techniques utilized in this research have proven effective for estimating vegetation expansion (natural and planned) at the Leslie Street Spit from 1974 to 2024. The land cover classifications, taking advantage of a wide variety of additional input combinations, produced overall classification accuracies ranging between 83.5% and 95.0%. NDVI and Tasseled Cap Greenness inputs performed best, acting as inputs to the most accurate land cover classifications 75% and 80% of the time, respectively. NDVI differencing proved effective for representing changes in vegetation cover on the evolving landform.

Over the 50-year study period, the total area of vegetation expansion is estimated at 213 ha (2,128,725 m2), with an average annual rate of 4.26 ha/year. The rates of vegetation expansion vary greatly across time intervals, with the greatest annual expansion at 9.90 ha/year between 1974 and 1978 and the least annual expansion at 0.972 ha/year between 2000 and 2005. Prior to 1995, when natural succession was the mechanism for vegetation expansion, approximately 84.8 ha (847,800 m^2) of growth occurred, at an average annual rate of 4.04 ha/year. From 1995 onward, when natural succession as well as habitat enhancement accounted for vegetation expansion, approximately 128 ha (1,280,925 m^2) of growth occurred, at an average annual rate of 4.42 ha/year.

The TRCA's determination to encourage habitat formation, along with natural succession from 1995 onward, is demonstrated by the increased average annual rate of expansion. However, by measuring and comparing vegetation expansion at the Leslie Street Spit over two time spans, the resilience of nature can be appreciated, from the peninsula's inception. "Nature chose the Spit" and brought forth a cosmopolitan array of plants and animals that inhabit the Spit as its *de facto* flora and fauna, offering "a hopeful narrative about how nature can flourish in, and contribute to, the well-being of twenty-first-century cities" (Kehm, 2020).

4.1 Limitations and Future Research

There are limitations associated with using NDVI for image differencing in this urban environment. Especially in coarser resolutions, mixed pixels can pose a significant problem – NDVI values become averaged and small vegetation details are not captured. Additionally, some built materials or barren land can produce NDVI values similar to sparse vegetation. NDVI is also sensitive to seasonal differences in vegetation health and timing – using only July image dates was an attempt at reducing these effects, but even within a single month, greenery can vary significantly. Some years see more precipitation than others and this affects plant vigour. NDVI measures green biomass, and some areas of forest on the Spit that have been damaged by cormorant nesting may have registered low NDVI values. However, the trees are still intact – unhealthy vegetation is still vegetation, and this may not be captured fully by NDVI.

A total of 20 clusters and 20 iterations was selected for classifying all imagery (land cover and difference images). These quantities adequately differentiated most cases of greenspace and built land. However, specifying a higher number of spectral clusters might have achieved greater class separation. Given the high volume of land cover classifications to produce (27) and difference image classifications (9), it was infeasible to increase the number of clusters – after specifying the maximum quantity of 255, a large proportion of those clusters were identified by the algorithm. For example, in the 2024 image, with original bands only as inputs, 157 of the 255 clusters contained pixels. Attempting to aggregate this quantity of clusters into information classes over potentially 36 images would be very challenging. The class separation challenge led to, for example, wetlands in Embayment D and Cell 1 being identified as greenspace while they may technically still be considered water. When higher quantities of clusters were tested, however, the wetlands issue persisted at least in part. Future research could involve experimenting with increasing the number of spectral clusters to more effectively differentiate classes.

Using 200 stratified random sample points for each accuracy assessment was insufficient to differentiate some of the more subtle classification differences, such as those involving Principal Components or Texture, and so four ties for best accuracy occurred out of the nine sets. It was impractical to classify every possible permutation of original bands plus the four input parameters for the nine images, so three classifications were chosen to assess for each timestep. Future research could involve increasing the number of random sample points used and the quantity of input permutations tested.

Exploring vegetation expansion at the Leslie Street Spit in nine time intervals presented raster coverage challenges – there were instances of both too much and too little representation. There are several areas where vegetation expansion rasters on the cumulative expansion map (Figure 22) of different time periods overlap. This may occur when areas of vegetation change transition back to built land and then back to vegetation at a later time. Overlaps also occur in areas where the change detection classification identifies, for example, a change from built land to sparse vegetation (and the classification at that area is greenspace) and in a subsequent time period, identifies a transition from sparse vegetation to lush vegetation (and the classification at that area is again greenspace). By grouping all vegetation into a single greenspace class, nuances in the quality and category of the vegetation cover are lost – vegetation in this study encompasses a diverse array of greenery, such as lush forests, sparse meadows, and even wetlands. Using a single greenspace class ignores this diversity. Future research could experiment with using two different classes for greenspace – sparse and lush – and/or more specific categories of vegetation such as forests, meadows, and wetlands.

Utilizing different spatial resolutions over variable time periods presents limitations. There are several gaps in the rasters on the cumulative expansion map that, by visual inspection of the

imagery, can largely be attributed to vegetation expansion occurring in the interim between 1983 and 1984 (transition from MSS to TM) and between 2011 and 2013 (transition from TM to OLI). Image availability issues in these time periods were a factor. In the case of OLI, the 30 m resolution was available (simply by skipping the pansharpening step) and could have ensured continuity with the TM sensor, but it was desirable to determine the effect that pansharpening would have on classification accuracy. In this case, pansharpening significantly improved classification accuracy over TM images on average, so there were both advantages and disadvantages to this choice. The gaps in raster coverage result in a slight underestimation of the total and annual vegetation expansion over the study period, but given the temporal scale of the research, the inability to resolve change over these short periods does not meaningfully affect the interpretation of multi-year land cover trends. Additionally, the pixel size inconsistency between MSS, TM, and OLI means that the same unit is not measured across time, and perceived "change" could simply be improved detection. The effects of mixed pixels are variable – at coarser resolution, pixels smooth out heterogeneity, and at finer resolution, pixels become more pure, revealing detail. In urban environments, small features such as trees, roads, and buildings that are invisible in MSS may be able to be perceived in TM or OLI. Thus, classification accuracy may improve simply due to resolution. Due to the scale dependency of spatial patterns, the same landscape will have a different measured structure across different resolutions. In reality, not only is time changing, but also the sensor, spatial resolution, and spectral signature. It becomes relevant to question the extent to which detected change is attributed to time or to the sensor.

REFERENCES

Alphan, H. 2013. Bi-Temporal Analysis of Landscape Changes in the Easternmost Mediterranean Deltas Using Binary and Classified Change Information. *Environmental Management* Vol. 51, Iss. 3, pp. 541-547.

Ataabadi, M.B., D. Chen, D. Pouliot, and T.S. Oluwadare. 10-13 June, 2024. Comparing the Performance of Different Classifiers for Urban Change Detection: A Case Study in Kingston, Ontario. Proceedings: *45th Canadian Symposium on Remote Sensing*. Halifax, NS.

Berberoğlu, S., A. Akin, P.M. Atkinson, and P.J. Curran. 2010. Utilizing image texture to detect land-cover change in Mediterranean coastal wetlands. *International Journal of Remote Sensing* Vol. 31, No. 11, pp. 2806-2811.

Cohen, W.B., T.A. Spies, R.J. Alig, D.R. Oetter, T.K. Maiersperger, and M. Fiorella. 2002. Characterizing 23 Years (1972-95) of Stand Replacement Disturbance in Western Oregon Forests with Landsat Imagery. *Ecosystems* Vol. 5, No. 2, p. 125.

Comber, A.J., P. Harris, and N. Tsutsumida. 2016. Improving land cover classification using input variables derived from a geographically weighted principal components analysis. *ISPRS Journal of Photogrammetry and Remote Sensing* Vol. 119, p. 359.

Congalton, R.G. 10-14 July, 1989. Considerations and Techniques for Assessing the Accuracy of Remotely Sensed Data. Proceedings: *12th Canadian Symposium on Remote Sensing Geoscience and Remote Sensing Symposium.* Vancouver, BC.

Coppin, P.R. and M.E. Bauer. 1996. Digital Change Detection in Forest Ecosystems with Remote Sensing Imagery. *Remote Sensing Reviews* Vol. 13, pp. 208-226.

Crist, E.P. and R.C. Cicone. 1984. A Physically-Based Transformation of Thematic Mapper Data—The TM Tasseled Cap. *IEEE Transactions on Geoscience and Remote Sensing* Vol. GE-22, No. 3, p. 259.

Esri. 2026. *ArcGIS Pro.* https://www.esri.com/en-us/arcgis/products/arcgis-pro/overview (accessed 25 Aug. 2025)

Ezaidi, S., A. Aydda, B. Kabbachi, O.F. Althuwaynee, A. Ezaidi, M.A. Haddou, I. Idoumskine, J. Thorpe, H-J. Park, and S-W. Kim. 2022. Multi-temporal Landsat-derived NDVI for vegetation cover degradation for the period 1984-2018 in part of the Arganeraie Biosphere Reserve (Morocco). *Remote Sensing Applications: Society and Environment* Vol. 27, p. 5.

Ferrato, L-J. and K.W. Forsythe. 2013. Comparing Hyperspectral and Multispectral Imagery for Land Classification of the Lower Don River, Toronto. *Journal of Geography and Geology* Vol. 5, No. 1, pp. 92-103.

Forsythe, K.W. 2004. Pansharpened Landsat 7 Imagery for Improved Urban Area Classification. *Geomatica* Vol. 58, pp. 23-27.

Forsythe, K.W., B. Schatz, S.J. Swales, L-J. Ferrato, and D.M. Atkinson. 2012. Visualization of Lake Mead Surface Area Changes from 1972-2009. *ISPRS International Journal of Geo-Information* Vol. 1, Iss. 2, p. 110.

Forsythe, K.W. and G. McCartney. 2014. Investigating Forest Disturbance Using Landsat Data in the Nagagamisis Central Plateau, Ontario, Canada. *ISPRS International Journal of Geo-Information* Vol. 3, Iss. 1, pp. 256-263.

Forsythe, K.W. and N.M. Waters. 2006. The Utilization of Image Texture Measures in Urban Change. *Photogrammetrie, Fernerkundung, Geoinformation* No. 4, pp. 289-290.

Forsythe, K.W. and R.D. Wheate. 2003. Utilization of Landsat TM and Digital Elevation Data for the Delineation of Avalanche Slopes in Yoho National Park (Canada). *IEEE Transactions on Geoscience and Remote Sensing* Vol. 41, No. 11, pp. 2678-2680.

Häme, T., I. Heiler, and J. San Miguel-Ayanz. 1998. An unsupervised change detection and recognition system for forestry. *International Journal of Remote Sensing* Vol. 19, No. 6, p. 1094.

Han, T., M.A. Wulder, J.C. White, N.C. Coops, M.F. Alvarez, and C. Butson. 2007. An Efficient Protocol to Process Landsat Images for Change Detection With Tasselled Cap Transformation. *IEEE Geoscience and Remote Sensing Letters* Vol. 4, No. 1, p. 147.

Healey, S.P., W.B. Cohen, Y. Zhiqiang, and O.N. Krankina. 2005. Comparison of Tasseled Cap-based Landsat data structures for use in forest disturbance detection. *Remote Sensing of Environment* Vol. 97, No. 3, p. 309.

Hemati, M., M. Hasanlou, M. Mahdianpari, and F. Mohammadimanesh. 2021. A Systematic Review of Landsat Data for Change Detection Applications: 50 Years of Monitoring the Earth. *Remote Sensing* Vol. 13, Iss. 15, pp. 2870-75.

Hough, M. 2004. Cities and Natural Process (2nd ed.). Routledge. New York, New York. 139-142pp.

Kauth, R.J. and G.S. Thomas. 1976. The tasseled cap — a graphic description of spectral-temporal development of agricultural crops as seen by Landsat. Proceedings: *2nd international symposium on machine processing of remotely sensed data*. West Lafayette, IN: Purdue University.

Kehm, W.H. 2020. Accidental Wilderness: The Origins and Ecology of Toronto's Tommy Thompson Park. University of Toronto Press. Toronto, Ontario. 33, 85-101pp.

Lu, D., P. Mausel, E. Brondízio, and E. Moran. 2004. Change detection techniques. *International Journal of Remote Sensing* Vol. 25, No. 12, pp. 2366-2382.

Mancino, G., A. Falciano, and M.L. Trivigno. 2025. Change Detection methods of forest expansion assessment in the last twenty years in the Mediterranean Basin. *iForest* Vol. 18, pp. 70-73.

Mancino, G., A. Nolè, F. Ripullone, and A. Ferrara. 2014. Landsat TM imagery and NDVI differencing to detect vegetation change: assessing natural forest expansion in Basilicata, southern Italy. *iForest* Vol. 7, pp. 75-79.

Masek, J.G., F.E. Lindsay, and S.N. Goward. 2000. Dynamics of urban growth in the Washington DC metropolitan area, 1973-1996, from Landsat observations. *International Journal of Remote Sensing* Vol. 21, No. 18, pp. 3477-3479.

PCI Geomatics. 2026. *Catalyst Professional.* https://catalyst.earth/solutions/catalyst-professional/ (accessed 25 Aug. 2025)

Pu, R., P. Gong, Y. Tian, X. Miao, R.I. Carruthers, and G.L. Anderson. 2008. Using classification and NDVI differencing methods for monitoring sparse vegetation coverage: a case study of saltcedar in Nevada, USA. *International Journal of Remote Sensing* Vol. 29, No. 14, pp. 3995-4009.

Shaban, M.A. and O. Dikshit. 2001. Improvement of classification in urban areas by the use of textural features: The case study of Lucknow city, Uttar Pradesh. *International Journal of Remote Sensing* Vol. 22, No. 4, pp. 571-591.

Shen, W., M. Li, C. Huang, X. Tao, S. Li, and A. Wei. 2019. Mapping Annual Forest Change Due to Afforestation in Guangdong Province of China Using Active and Passive Remote Sensing Data. *Remote Sensing* Vol. 11, Iss. 5, p. 491.

Sun, H., K.W. Forsythe, and N.M. Waters. 2007. Modelling Urban Land Use Change and Urban Sprawl: Calgary, Alberta, Canada. *Networks and Spatial Economics* Vol. 7, No. 4, p. 354.

Toronto and Region Conservation Authority. 2020. *Tommy Thompson Park.* https://tommythompsonpark.ca/ (accessed 26 Mar. 2025)

Toronto and Region Conservation Authority. 2024. A History of Tommy Thompson Park. *Toronto and Region Conservation Authority.* May 2, 2024. Available online: https://trca.ca/news/tommy-thompson-park-history/

United States Geological Survey (USGS). 2025. *What are the best Landsat spectral bands for use in my research?* https://www.usgs.gov/faqs/what-are-best-landsat-spectral-bands-use-my-research (accessed 25 Aug. 2025)

United States Geological Survey (USGS). 2026. *EarthExplorer.* https://earthexplorer.usgs.gov/ (accessed 2 Apr. 2025)

Viana, C.M., I. Girão, and J. Rocha. 2019. Long-Term Satellite Image Time-Series for Land Use/Land Cover Change Detection Using Refined Open Source Data in a Rural Region. *Remote Sensing* Vol. 11, Iss. 9, p. 1108.

Wilson, E.H, and S.A. Sader. 2002. Detection of forest harvest using multiple dates of Landsat TM imagery. *Remote Sensing of Environment* Vol. 80, Iss. 3, pp. 391-392.

Zewdie, W. and E. Csaplovies. 2015. Remote Sensing based multi-temporal land cover classification and change detection in northwestern Ethiopia. *European Journal of Remote Sensing* Vol. 48, Iss. 1, p. 125.